UPPSALA
UNIVERSITET

Digital Comprehensive Summaries of Uppsala Dissertations from the Faculty of Science and Technology 231

Radar Probing of the Sun

MYKOLA KHOTYAINTSEV

ACTA
UNIVERSITATIS
UPSALIENSIS
UPPSALA
2006

ISSN 1651-6214
ISBN 91-554-6681-8
urn:nbn:se:uu:diva-7192

Dissertation presented at Uppsala University to be publicly examined in Polhemsalen, Ångström Laboratory, Lägerhyddsvägen 1, Uppsala, Saturday, November 4, 2006 at 10:00 for the degree of Doctor of Philosophy. The examination will be conducted in English.

Abstract
Khotyaintsev, M. 2006. Radar Probing of the Sun. Acta Universitatis Upsaliensis. *Digital Comprehensive Summaries of Uppsala Dissertations from the Faculty of Science and Technology* 231. 83 pp. Uppsala. ISBN 91-554-6681-8.

This thesis is dedicated to the theory of solar radar experiments. The Sun exhibits a variety of interesting and complicated physical phenomena, examined mainly through analysis of its radiation. Active solar probing by radar provides an alternative possibility to study the Sun. This concept was tested originally in the 1960's by solar radar experiments at El Campo, Texas, but due to an insufficient level of technology at that time the experimental results were of a poor quality and thus difficult to interpret. Recently, the space weather program has stimulated interest in this topic. New experimental proposals require further development of the theory of solar radar experiments to meet the current knowledge about the Sun and the modern level of technology.

Three important elements of solar radar experiments are addressed in this thesis: i) generation of wave turbulence and radiation in the solar corona, ii) propagation of the radar signal to the reflection point, and iii) reflection (scattering) of the incident radar signal from the Sun.

It is believed that the radio emission of solar type II and III bursts occurs due to conversion of Langmuir waves, generated by electron beams, into electromagnetic radiation (plasma emission mechanism). The radar signal propagating through the emission source region can get scattered by the Langmuir turbulence and finally deliver the observer insights of the physics of this turbulence. Such process of scattering is considered in this thesis in the weak turbulence limit by means of the wave-kinetic theory. Scattering frequency shifts, scattering cross-sections, efficiency of scattering (the coefficient of absorption due to scattering), optical depths, and the spectra of the scattered signal are estimated.

Type II solar radio bursts are known to be associated with the electron beams accelerated by interplanetary shocks. From their dynamic spectra the properties of the shocks and regions in the vicinity of the shock are usually inferred by assuming a plasma emission mechanism. *In situ* observations of the source region of type II burst, presented in this thesis, suggest that an additional emission mechanism may be present. This mechanism is related to energetic particles crossing the shock front, known in electrodynamics as transition radiation.

Plasma density fluctuations are known to scatter radio waves and thus broadening their angular dispersion. In the thesis this process is studied in the solar wind and terrestrial electron and ion foreshocks on the basis of *in situ* observations of density fluctuations. It is shown that the angular broadening of the radar signal is negligible in this regions.

The results of this thesis can be applied for the preparation of future solar radar experiments and interpretation of experimental data.

Keywords: solar radar, active experiments, space physics, solar corona, plasma

Mykola Khotyaintsev, Department of Astronomy and Space Physics, Box 515, Uppsala University, SE-75120 Uppsala, Sweden

ISSN 1651-6214
ISBN 91-554-6681-8
urn:nbn:se:uu:diva-7192 (http://urn.kb.se/resolve?urn=urn:nbn:se:uu:diva-7192)

Cover illustration: North-South arm of the UTR-2 radio telescope, located near Kharkiv, Ukraine.

A method is more important than a discovery,
since the right method will lead to new
and even more important discoveries.

L. D. Landau

List of Papers

This thesis is based on the following papers, which are referred to in the text by their Roman numerals.

I **Combination scattering by anisotropic Langmuir turbulence with application to solar radar experiments,**
Khotyaintsev, M., Mel'nik, V. N., Thidé, B., Konovalenko, O. O.,
Solar Physics, 234:169-186, 2006.

II **Radar detection of interplanetary shocks: scattering by anisotropic Langmuir turbulence,**
Khotyaintsev, M., Mel'nik, V. N., Thidé, B.,
Submitted to *Advances in Space Research*, 2006.

III **Scattering of radio waves by density fluctuations in the solar wind and terrestrial foreshock,**
Khotyaintsev, M., Khotyaintsev, Y., Krasnosel'skikh, V.,
Submitted to *Annales Geophysicae*, 2006.

IV **In situ observation of a type II solar radio burst source region: a new generation mechanism,**
Khotyaintsev, M., Khotyaintsev, Y., Krasnosel'skikh, V., Mühlbachler, S.
Submitted to *Astrophysical Journal Letters*, 2006.

Contents

1. Introduction

Everyone knows how powerful a radar can be in hands of a policeman,
but few know how valuable it can be in hands of a scientist.

A standard method of investigating an unknown object in a physics laboratory is to determine its scattering properties when exposed to a collimated beam of particles or electromagnetic waves. This approach is applied in the radar (radio detection and ranging) astronomy to study celestial objects, in meteorology, ionospheric physics, and many other fields. A radar transmits a beam of radio waves in the direction defined by the antenna system and records a signal reflected (scattered) by objects lying in the radar beam path. The energy flux in the transmitted beam decreases as the square of the distance from the transmitter, and the reflected energy flux falls in the similar way. Consequently, the overall echo power falls off as the fourth power of the distance. Therefore, it seems that study of objects by radar will be forever confined to the solar system.

The Sun exhibits a verity of physical phenomena, some of which are still not at all or only barely understood, such as coronal heating and acceleration of the solar wind. The Sun is studied mainly on the basis of its radiation. The idea to use a radar to study the Sun appeared in the 1940's along with the first successful experiment in detecting a space object, the moon [68, 5]. The theoretical background for solar radar experiments was laid out by Ginzburg (1946) [23], Kerr (1952) [48], and Bass and Braude (1957) [4], who estimated the expected echo and necessary radar parameters. The first reflections from the Sun were claimed to be observed by a group at Stanford University in 1959 using a radar at 25 MHz [18]. The first systematic radar experiments were conducted from 1961 to 1969 by an MIT group led by Jesse James at the dedicated solar radar facility build at El Campo, Texas [42, 34]. All other solar radar experiments until now were unsuccessful. Thus, the experiments performed with the El Campo radar remain the only source of solar radar echo data to date.

The results obtained at the El Campo were to a large extent unexpected. Initially, it was assumed that echoes would come from a layer of a zero refractive index (the so-called specular reflection), which corresponds to the altitude of about 1.6 $R_\odot$ in the solar corona and would have intensity, expressed in scattering cross-sections, of about 1.5 $\pi R_\odot^2$, where $R_\odot$ is the radius of the Sun. However, the observed echoes were coming from different altitudes, from $-2.6\ R_\odot$ (reflection from the back side of the Sun) up to 5 $R_\odot$.

The observed cross-section values varied significantly from day to day, ranging from less than $\pi R_\odot^2$ to up to several hundreds of $\pi R_\odot^2$. It became apparent that the specular reflection model was not sufficient to explain the observations, and that the echo signal may result from more complex wave-plasma interactions in the turbulent solar corona [30].

Scattering by wave turbulence is routinely studied in laboratory and ionospheric radar experiments. The latter are very similar to solar radar experiments and thus might be very useful. Both the ionosphere and the solar corona have magnetic fields and gradients of density. The wave turbulence in the ionosphere can be excited by the natural phenomena, *e.g.* by field-aligned currents, as well as by the manmade, *i.e.* transmitting of a powerful HF (high frequency) electromagnetic wave, so called heating experiments. In the solar corona the wave turbulence can be excited by an electron beam accelerated on the Sun or interplanetary shock. Existence of such electron beams in the solar corona is manifested by the radiation of the excited wave turbulence, known as solar radio bursts.

The space weather program[1] recently stimulated interest in solar radar experiments, with a major goal of early detection of the Coronal Mass Ejections (CMEs), traveling towards the Earth. Such geoeffective CMEs can have a severe impact on the life of astronauts, may damage satellites, cause intense geomagnetic storms, which in their turn can lead to the damaging of the power lines, and black-outs of vast territories [80]. Recent proposals of new radar experiments can be found in the references [87, 13, 78]. It is likely that new radar observations with modern techniques of transmission, reception, and processing of signal, combined with modern optical, UV, and X-ray observations, will make a significant contribution to our understanding of the physics of the Sun.

This thesis comprises four papers. Papers I and II are devoted to the problem of radar scattering by an anisotropic Langmuir turbulence in the corona. Paper III considers the impact of plasma density fluctuations on propagation of radar signals, and Paper IV introduces a new emission mechanism of solar type II radio burst.

The purpose of the first part of the thesis is to present a background for the successful reading of the papers it is comprised of. The next chapter introduces the reader to the Sun, its structure, "quiet" and sporadic (radio burst) radio emission, and emission mechanisms. Chapter 3 gives an overview of solar radar experiments and the main results. An overview of the theory of solar radar experiments is presented in Chapter 4. Chapter 5 contains a summary of the papers.

[1] See for example `http://www.spaceweather.com`

2. The Sun and its corona

2.1 Overview

The Sun is a the closest and, by far, the most important star for life on the Earth. From the Earth it might look small (0.53° or 32 arcmin), but this is only because it is located at the distance of 150 million kilometres (one astronomical unit [a.u.]) from the Earth. For light it takes about eight minutes to travel this distance.

All of the Sun's energy is produced in the form of γ-rays by the fusion of hydrogen into helium, in the dense, high-temperature *core*, which extends from the centre of the Sun to about one quarter of the radius of the visible disk, $R_\odot \approx 6.9 \times 10^{10}$ cm.

Nuclear reactions cannot occur in the cool, less dense regions outside the core. Thus, no energy is produced there. The energy from the core is transported outward through a number of more or less concentric shells, characterized by different mechanisms of energy transport. They are called the *radiative zone* and the *convective zone*.

In the inner shell, called the *radiative zone*, the energy is transported outward by radiative diffusion. Photons are traveling in a random walk, being continuously absorbed and re-emitted by plasma particles on their way. This process leads to a downshifting of photons to lower energies so that their wavelength becomes longer. Because of the continuous scattering in the radiative zone, it takes about 200 000 years for radiation to reach the bottom of the *convective zone* (at $\approx 0.71 R_\odot$).

The plasma temperature decreases from 1.55×10^7 K in the centre to some 2×10^6 K at the bottom of the convective zone. At this point the temperature gradient becomes too steep for the plasma to remain in static equilibrium and convective motion sets in, becoming the dominant mode of energy transport. The heated plasma carries energy through the convective zone, from the bottom to the top, in about 10 days. Then it cools, by radiating out into space, sinks back down to become heated and rise again. This plasma motion, in combination with the solar rotation, leads to the generation of Sun's magnetic field.

The convective zone is covered by a thin (about 500 km thick) shell, called the *photosphere* (after the Greek word for light "photo"), at a temperature of 5780 K. At this point the outer layers of the Sun become transparent to optical light, and the most of the Sun's energy finally escapes out into space. White light observations of the photosphere show the underlying convecting process

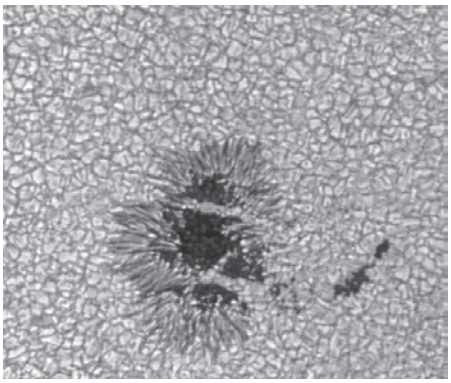

Figure 2.1: The sunspot surrounded by the granulation (chromosphere). Observed at 468 nm by P. N. Brandt and G. W. Simon at the Swedish Vacuum Solar Telescope (SVST) at La Palma with the support of G. Scharmer. Adapted from http://www.kis.uni-freiburg.de/∼pnb/spot/snap3.gif

as bubbling granulation, a coarse cell structure with a mean size of 1300 km (Figure 2.1). Larger and deeper convection cells, called *the supergranules*, are about 35000 km across; but they are not visible in white light.

Most of the time the photosphere is pitted with dark spots, called *sunspots* (Figure 2.1). The largest of them can be many times larger then the Earth and may be observed with an unaided eye. Sunspots appear to be dark because their temperature are some 2000 degrees lower than the temperature of the photosphere. Exceptionally bright patches are also present in the chromosphere, and they are called *faculae*, from the Latin word for "little torches." Faculae are associated with strong magnetic fields. The magnetic field in the center of the sunspot is very strong (~ 0.1 T) and nearly radial. It weakens (down to ~ 0.01 T) and inclines strongly on the edge of the sunspot. The strong magnetic field of the sunspot prevents the upward convection and outward flow, keeping the region cooler than the surrounding plasma.

Sunspots normally occur in pairs of opposite magnetic polarity which are joined by magnetic loops and rise into the overhead solar atmosphere. These magnetic loops confine the hot plasma above the sunspot pairs and can be observed in ultraviolet (UV) or X-ray, because they usually dominate the solar radiation. Sunspots and the corresponding magnetic loops are also called *active regions*. A magnetic loop changes its topology continuously. Sometimes it may release its energy in a sudden and catastrophic explosion, called a *solar flare*.

Solar activity changes periodically with a 11-year cycle. Various approaches exist for measuring the activity and various indices have been devised to characterize this activity quantitatively. The simplest, but nevertheless one of the best activity index is *the Wolf sunspot number R*, given by

$$R = k(10g + s), \tag{2.1}$$

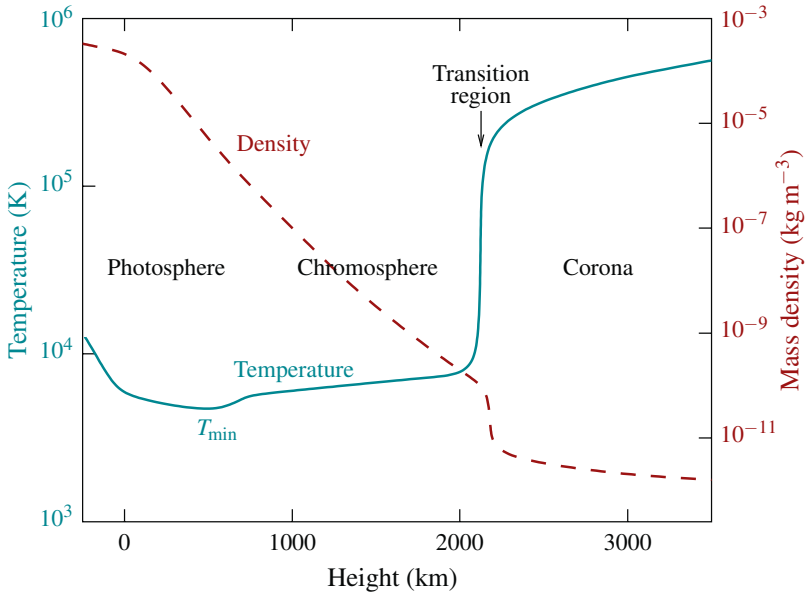

Figure 2.2: Sketch of the temperature and gas mass density in the solar photosphere, chromosphere, and lower corona, including the transition region [87].

where g is a number of sunspot groups, s is the total number of sunspots in all the groups on one and the same day, and k is a factor based on the estimated efficiency of the observer and the telescope used.

Just above the photosphere lies a relatively thin layer, called the *chromosphere* (from *chromo*, the Greek word for "colour"). It is about 2500 km thick and quite faint compared to the photosphere. A small temperature rise in the chromosphere is accompanied by roughly a millionfold drop in density (Figure 2.2). Because of this, absorption lines are not formed any more, but in contrary the gas starts to strongly emit spectral lines. There are more than 3500 known lines, mostly in optical and UV range. The chromosphere is jagged, irregular and by no means smooth. It consists of needle-shaped *spicules*, about 2 km in width, which shoot up to the heights of about 25 000 km at speeds of about 20 km/s.

Still higher, above the chromosphere, within a narrow *transition region* of only a few hundred kilometers, the temperature rises dramatically from 10^4 K at the top of the chromosphere to a more than 10^6 K in the *corona*. The density drops down as the temperature increases, in such a way as to keep the gas pressure spatially constant. The paradox of the corona being hundreds of times hotter then the underlying chromosphere is still unresolved. Further away, the coronal temperature and density slowly decreases, reaching some 1.4×10^5 K and a few particles per cubic centimetre near the Earth. The coronal plasma is not static, but flows continuously outward from the Sun. This phenomenon is called the *solar wind*. Spacecraft missions detect the average solar wind speed of about 400 km/s near the Earth. However, sometimes the speed may

exceed 800 km/s. This has been measured by spacecraft in the regions of open magnetic field lines of the Sun, called the *coronal holes*.

2.2 Plasma density in the corona

The plasma density in the corona drops as the distance from the Sun increases. Here we present the most popular models which describe the radial dependence of the electron plasma density in the corona, assuming anisotropy. The reader may also consult more sophisticated models, which take into account the dependence on heliographic latitude [91, 90, 8].

One of the oldest but nevertheless very widely used model is the Allen's revision [1] of Baumbach's model which is based on the intensity of the white light of the corona

$$N_{\mathrm{e}}(r) = 10^8 \times \left[1.55 \left(\frac{r}{R_\odot} \right)^{-6} + 2.99 \left(\frac{r}{R_\odot} \right)^{-16} \right] \quad \mathrm{cm}^{-3} \tag{2.2}$$

[94, 28]. It is referred as the *Baumbach-Allen* model.

Another popular model is the *Newkirk* model [71], which gives the electron density as

$$N_{\mathrm{e}}(r) = 4.2 \times 10^4 \times 10^{4.32 R_\odot / r} \quad \mathrm{cm}^{-3}. \tag{2.3}$$

The most recent and advanced model is the the heliospheric density model of *Mann et al.* [55]. In the inner region of the corona where the solar wind velocity is subsonic (much smaller than the ion sound velocity) this model has an analytical solution in the form of a barometric formula

$$N_{\mathrm{e}}(r) = N_{\mathrm{e}\odot} \exp \left[\frac{A}{R_\odot} \left(\frac{R_\odot}{r} - 1 \right) \right], \tag{2.4}$$

with $N_{\mathrm{e}\odot} = N_{\mathrm{e}}(r = R_\odot)$ and $A = G\mu m_{\mathrm{p}} M_\odot / \kappa_{\mathrm{B}} T$, where T is the temperature of the corona, κ_{B} is Boltzmann's constant, μ is the relative mean molecular mass, assumed to have the value 0.6 [74], m_{p} is the proton mass, G is the gravitational constant, and $M_\odot$ is the mass of the Sun. Actual values of $N_{\mathrm{e}\odot}$, A, and the altitude where the solar wind becomes supersonic for different temperatures of the corona T are given in Table 2.1. Note that the Newkirk model corresponds to the Mann model with the temperature of 1.4×10^6 K.

The local plasma frequencies in the solar corona calculated from the density given by the three models presented are plotted in Figure 2.3.

2.3 Radio emission of the Sun

The Sun and its atmosphere radiate in a broad electromagnetic spectrum. Radiation from γ-rays to radio, come mostly from the regions containing dense

Table 2.1: *Electron number density $N_{e\odot}$, the radius, where the solar wind becomes supersonic R_c, and coefficient A for different temperatures of the corona T [55].*

T (10^6 K)	$R_c/R_\odot$	$N_{e\odot}$ (m^{-3})	A (m)
1.0	6.91	5.14×10^{15}	9.64×10^9
1.4	4.90	1.61×10^{14}	6.87×10^9
2.0	3.43	1.40×10^{13}	4.82×10^9

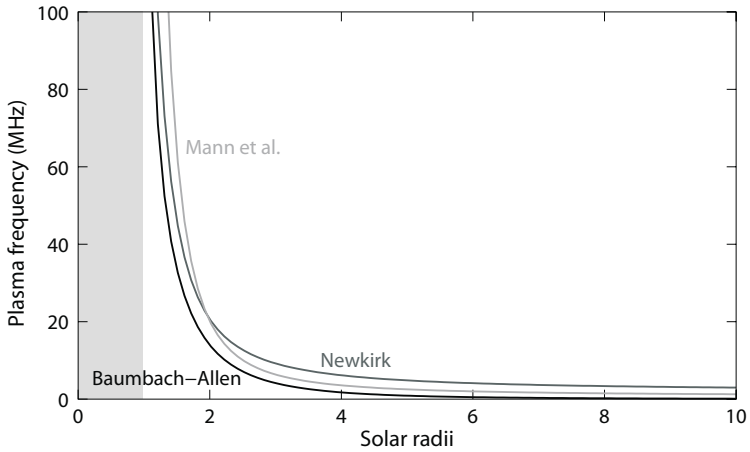

Figure 2.3: The radially dependent plasma frequency of the solar corona at a temperature of 1.0×10^6 K according to the models of *Mann et al.*, Eq. (2.4), *Baumbach-Allen*, Eq (2.2), and *Newkirk*, Eq. (2.3). The grey strip covers 1 $R_\odot$.

matter associated with the visible Sun — the photosphere and chromosphere, the metre radiation comes from the lower corona, and longer wavelengths radiation comes mainly from the upper corona which extends into interplanetary space. Here we will mostly concentrate on the emission in the radio frequency band starting from metre wavelength (300 MHz) and longer and mechanisms of its generation.

The discovery of metrewave radiation from the Sun was very exciting. In February 1942, two circumstances combined: the largest sunspot group ever recorded appeared on the face of the Sun, and Britain, at war with Germany, was constantly monitoring the skies for hostile aircraft with the aid of a recently developed metre-wavelength radar. And it so happened that strong, noise-like and highly variable jamming, reported by radar operators, was traced to electromagnetic radiation from the Sun. The discovery was made by J. S. Hey, who led the British Army Operational Research Group which investigated the jamming. Hey noted the presence of a major solar flare at the

time. The discovery was kept secret until after the war, and in 1945 this first well-documented example of metrewave bursts and their association with solar flares was published [2].

Much of the Sun's radio radiation is due to individual electrons when they are accelerated either because of collisions with ions (free-free emission or bremsstrahlung) [82, 56] or because of spiraling in a magnetic field (gyromagnetic emission) [56].

Bremsstrahlung ("breaking radiation" in German) or free-free emission is an incoherent process and is the basic emission process for a plasma of relatively low temperature $\leqslant 10^6$ K. It is important for the quiet Sun. The inverse process, free-free absorption occurs when electrons begin to oscillate in resonance with electric field of a wave and then electron-ion collisions destroy the oscillation; dumping of radio waves in the corona due to this process is considered in Section 4.2.

Gyromagnetic emission comes at harmonics of the electron gyrofrequency ω_{ce}, and for this emission to escape out into space, its frequency should exceed the local electron plasma frequency ω_{pe}. Although gyro emission is usually treated as a single-particle incoherent process — and this is the case of most interest for solar radio physics — it is possible for gyro emission to occur in a collective way, *e.g.* in electron-cyclotron maser emission.

Another coherent mechanism of plasma emission is often called *plasma emission* [27, 66], since in involves the generation of radiation near the local plasma frequency (fundamental plasma emission) or its harmonics. Plasma emission occurs in solar metre-wave radio bursts, which we will describe later in this Section. The most familiar is the type III solar radio burst, which is attributed to a subrelativistic electron beam travelling along open magnetic field lines out of the Sun. Plasma emission is necessarily a multistage process, unlike the direct emission process such as thermal and nonthermal synchrotron radiation and electron-cyclotron maser instability. Plasma emission process consists of two steps: i) the generation of plasma turbulence that cannot escape from the source and ii) its partial conversion into escaping radiation through a secondary nonlinear process.

The appearance of the quiet solar atmosphere at radio wavelengths is governed by the plasma parameters (temperature, density, and magnetic field strength) and the radiation mechanisms that generate radio emission (free-free emission, gyromagnetic emission, and plasma emission). Figure 2.4 shows the height versus frequency of three characteristic frequencies — the plasma frequency, the gyrofrequency, and the frequency at which free-free (bremsstrahlung) emission reaches unity optical depth.

2.3.1 Plasma emission mechanisms

As the plasma emission mechanism involves the generation of wave turbulence we will describe it in detail. The first theory for plasma emission was

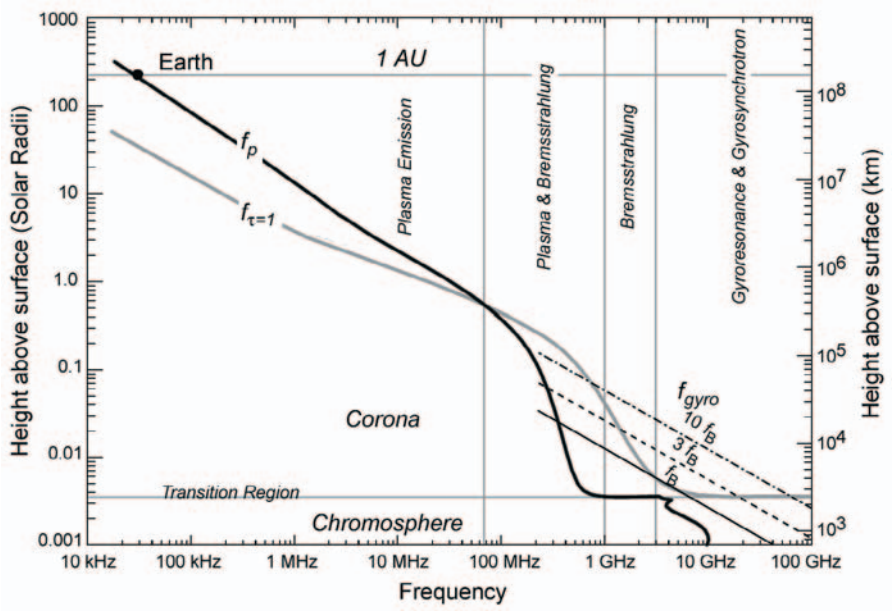

Figure 2.4: The highest curve shows the emission mechanism that will dominate at different frequencies in the solar atmosphere. The curves are based on the dependence of different emission mechanisms on the plasma parameters of temperature, density, and magnetic field strength [21].

proposed by Ginzburg and Zheleznyakov (1958) [27] for type III bursts. At the time this theory was proposed it was accepted that type III bursts involve emission of transverse waves at the fundamental ($\omega = \omega_{pe}$) and second harmonic ($\omega = 2\omega_{pe}$), and that the emission is excited by a beam of electrons that is accelerated at the Sun, often in solar flares. A variant of this theory is outlined in Figure 2.5. Although the details of the plasma physics have been updated, the basic ideas are unchanged.

The first step in the production of plasma emission is the generation of Langmuir waves. Langmuir waves are excited by bump-in-tail instability due to a beam of suprathermal electrons with velocity v_b, which creates a positive derivative of the electron distribution function $df(v_z)/dv_z > 0$. For $\omega_{ce}/\omega_{pe} < 1$ the growth of Langmuir waves is maximal for propagation along the beam direction ($\theta = 0$) with phase speed $v_{ph} \lesssim v_b$, and the fast growth is confined to a small range of θ and v_{ph}. The mutual interaction of the waves and the particles is described by a pair of quasilinear equations. The feedback on the distribution of particles, referred as quasilinear relaxation, involves smoothing out of the bump to form a plateau $df(v_z)/dv_z \approx 0$. It was pointed out by Sturrock (1964) [84] that in a homogeneous beam-plasma model the beams should propagate only a few kilometre before losing all their energy to the Langmuir waves. However, the electron beams were known to propagate through the corona and some beams were known to propagate beyond the orbit of

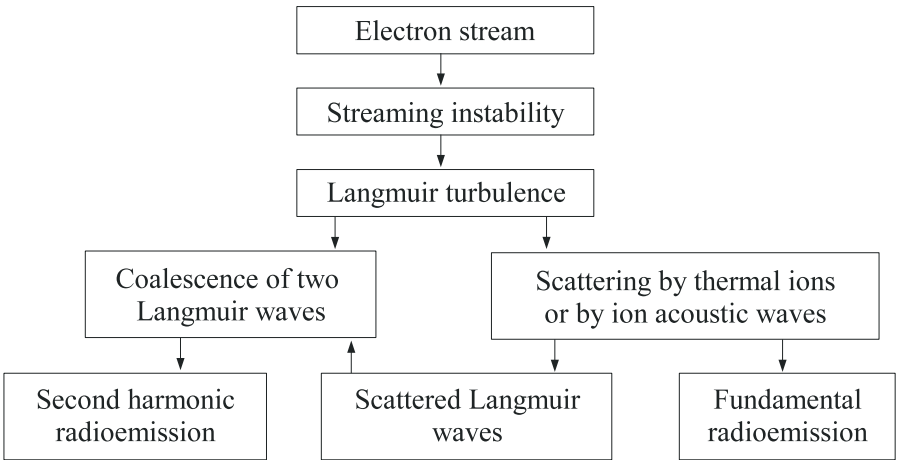

Figure 2.5: Steps in the theoretical description of emission of electromagnetic radiation by an electron stream in a plasma.

the Earth, still generating Langmuir waves and radiation. A variety of theories have been proposed to explain beam stabilization. A first set of theories is based on the saturation of the instability due to the inhomogeneity in the stream. A second set considers the influence of the ambient density fluctuations on the growth rate of the beam-plasma instability, *i.e.* quasi-linear relaxation of the electron stream to marginal stability. A review of these theories can be found in Ref. [69].

Nonlinear processes will cause partial conversion of the energy of the Langmuir waves into electromagnetic radiation. In fact, such nonlinear processes were considered as an additional mechanism to the nonlinear saturation of the beam-driven Langmuir instability. There are at least four known mechanisms of conversion of Langmuir waves into plasma emission. They include i) wave-particle interaction involving both spontaneous and induced scattering of Langmuir waves into electromagnetic radiation by thermal ions [27, 3, 86], ii) wave-wave interactions involving either merging of Langmuir wave with low-frequency waves to produce electromagnetic waves or, alternatively, the decay of Langmuir waves into low-frequency and electromagnetic waves [85, 64, 65, 86], iii) strong turbulence involving emission of electromagnetic waves by a Langmuir soliton [29] or incoherent emission due to scattering of long-wavelength Langmuir waves on collapsed Langmuir cavitons [50], and vi) direct coupling between Langmuir and electromagnetic waves due to large-scale gradients or local inhomogeneities in the electron density [94, 63].

At present the most popular nonlinear process for the generation of type II and III radio emission include ion-sound waves. The process that can lead to fundamental emission are the $l + s \rightarrow t$ (coalescence) and $l \rightarrow t + s$ (decay), where l refers to a Langmuir wave, s to an ion-sound wave, and t to transverse wave. The primary Langmuir wave may also decay into a secondary Langmuir

wave in the process $l \rightarrow l' + s$. The coalescence of the primary and secondary Langmuir wave $l + l' \rightarrow t$ can then produce the second harmonic emission. However, ion-sound waves can only exist in plasmas with $T_e \gg T_i$, otherwise they are heavily damped. Therefore the accepted nonlinear mechanism of generation of plasma emission including ion-sound turbulence can only work in the regions where $T_e \gg T_i$. For instance in the solar corona $T_e \sim T_i$, while in the fast solar wind $T_e/T_i \sim 3-5$.

The presence of a magnetic field extends the wave modes that can participate in the coalescence and decay processes. For example, upper-hybrid, Bernstein or Z mode waves can replace the l waves; lower-hybrid, Alfvén or whistler waves can replace the s waves, and O mode or X mode waves can replace of the t waves.

2.3.2 Solar radio bursts

Radio emission from the Sun is highly variable, and is often much brighter then can be expected in terms of thermal radiation from the solar corona. The various kinds of nonthermal radio emission are called solar radio bursts. The bursts discussed in this section are at decimetrewave ($f \sim 0.3-3$ GHz) and metrewave or longer ($f \lesssim 300$ MHz), here f is the frequency of observation, which is related to the wavelength λ as $\lambda = c/f$. Decimetre bursts are generated low in the corona, metre bursts at heights $\sim 1\,R_\odot$ above the Sun's surface and kilometre bursts (observed from spacecraft) originate in the interplanetary medium (IPM). Emission at higher frequencies in the radio range (mm and microwaves at $\gtrsim 3$ GHz) is related to solar flares. The classification of radio burst is based primarily on its appearance on a dynamic spectrum, which exhibits f versus time t with the intensity of emission represented by a gray (or colour) scale (Figure 2.6). Important characteristics of bursts are their drift rate df/ft, their bandwidth Δf (at fixed t), their duration Δt (at fixed f), harmonic structure and other fine structures.

Metre bursts were originally classified (in 1950) into three types, denoted as type I, type II, and type III, according to their appearance on a dynamic spectrum. Later (ca 1960) this classification was extended to include type IV and V bursts. Detailed investigation of bursts at decimeter wavelength started in the late 1970s. We present this classification below.

Type I emission

Characteristics: Type I emission (Figure 2.6) is not associated with flares, but occurs in storms that can last from hours to days. The term type I burst was applied to the individual short-duration ($\sim$ 1s) narrow-band ($\Delta f/f \approx 0.025$) bursts f which metre-wavelength storms are composed. These storms were accordingly called type I storms. Type I emission is strongly ($\sim 100\%$) circularly (O mode) polarized, has high brightness temperature (from 10^7 to 10^9 K), and contains only fundamental (F) emission and no harmonic (H) components.

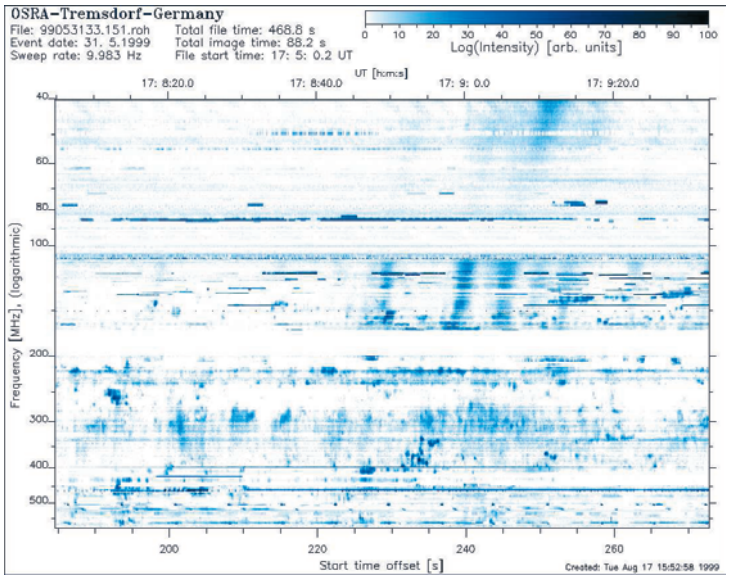

Figure 2.6: Solar radio noise storm. OSRA Solar Radio Observatory Potsdam-Tremsdorf, Germany. May 31, 1999. Adapted from http://www.aip.de/groups/osra/gallery/99053133_sp4.gif.

The bursts can drift to either higher of lower frequencies, with most bursts having negligible drift.

Interpretation: The short duration of the individual bursts suggests local acceleration of electrons to a few times the thermal energy. It is generally accepted that type I bursts must be some form of fundamental frequency plasma emission. This hypothesis explains important observed characteristics of type I storms, notably the high brightness temperature and strong O mode polarization. The long life of a storm points to continuing local energy release in the source region, which is probably related to magnetic field recombination after new flux intrudes into existing fields.

Type II bursts

Characteristics: Type II bursts (Figure 2.7) show a slow drift from high to low frequencies with a rate of $\lesssim 1$ MHz s^{-1}, often with a fundamental (F) ($\omega = \omega_p$) and harmonic (H) ($\omega = [1;2;3;\ldots] \times \omega_p$) structure. The instantaneous bandwidth may be as narrow as a few Megahertz, but this is not always the case. The starting frequency of the fundamental component is usually < 150 MHz, although starting frequencies as high as 500 MHz have been observed. Type II bursts are sometimes seen in the interplanetary medium, although most fade from view at ~ 1 MHz. With the exception of the very long-lived interplanetary events, the duration of a typical type II burst is 5 to 15 min. Many of the bursts show a band splitting in which the F and/or H component splits into two or multiple-lane structures (Figure 2.8). Some bursts exhibit

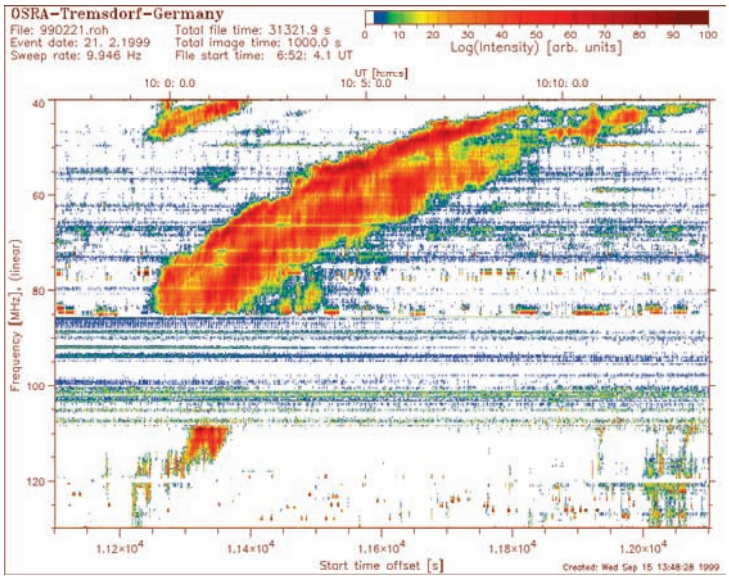

Figure 2.7: Type II burst with fundamental-harmonic structure and band-splitting. OSRA. February 21, 1999. Adapted from http://www.aip.de/groups/osra/gallery/990221_4.gif.

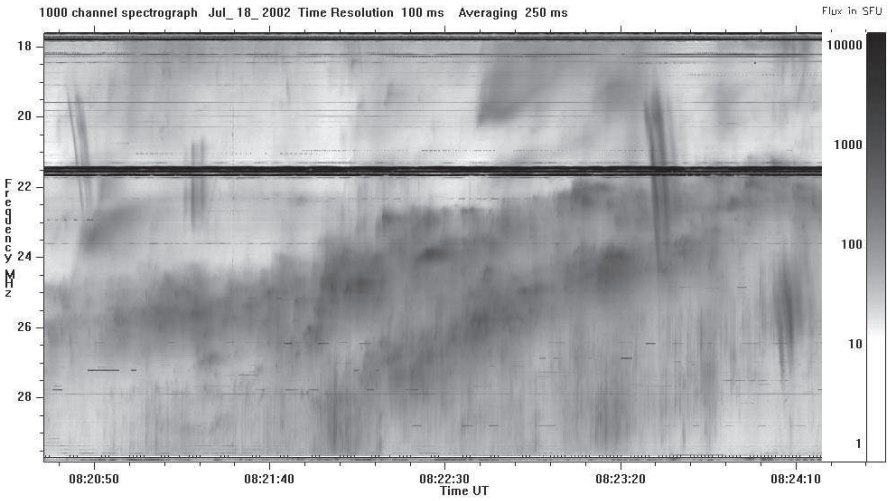

Figure 2.8: Band-splitting type II burst with different drift rates observed at the radio telescope UTR-2 (Ukrainian T-shape Radio telescope, second modification) [61].

herringbone structure in which type III like bursts emanate from a “backbone” of emission, and propagate either to lower and/or to higher frequencies (Figure 2.9). This gives the appearance of a fish bone on the dynamic spectrum, hence the name.

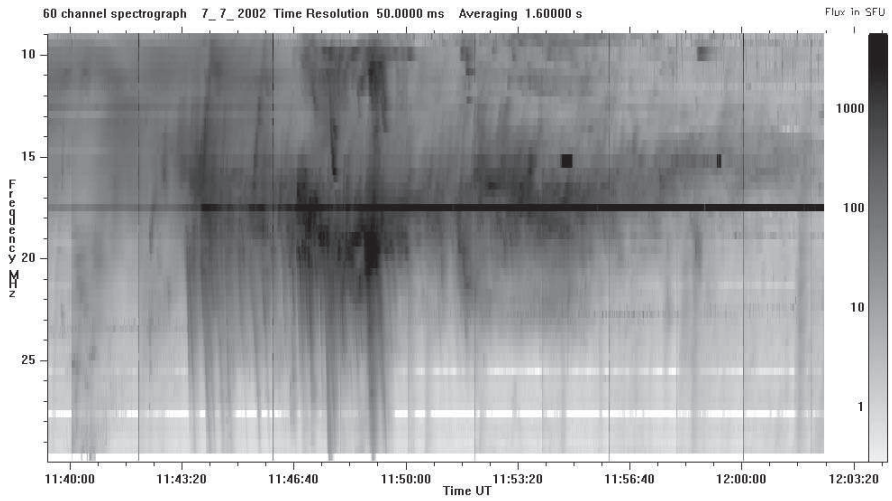

Figure 2.9: Type II burst with a herringbone structure and a waving backbone observed at the UTR-2 [61]. Fundamental radio emission of this burst is probably visible close to 10 MHz.

Early observations showed that the ordinary type II bursts are usually unpolarized or only weakly polarized. However, the herringbone structure is some bursts was found to be quite strongly polarized, e.g. up to 70%.

Interpretation: Type II burst is caused by a shock wave propagating from the low corona into interplanetary medium. This explains the slowly drifting feature in the dynamic spectrum. It is widely accepted that the radio emission itself occurs as a final step in a series of physical processes: initiation of the shock, particle acceleration, generation of plasma waves, and finally conversion of plasma waves into electromagnetic waves (plasma emission mechanism). In Paper IV we suggest an additional emission mechanism, which is related to crossing of the shock by energetic particles, known in electrodynamics as transition radiation (see Section 2.5). The herringbone structure in type II bursts is explained by the escape of the electrons upstream and downstream from the shock front. Early split bands interpretations involved magnetic splitting or Doppler splitting. Neither is satisfactory. Magnetic splitting in some cases requires unacceptably strong magnetic fields, and Doppler splitting requires a current which would cause electrons to flow at unacceptably high speeds relative to the ions in a laminar shock model. Two other alternative models have been proposed: emission from different parts in the shock front, or emission from in front and behind the shock front. It is still not possible to make a definite choice between two models.

Type III and related bursts

Characteristics: Type III bursts (Figure 2.10) occur over the frequency range 1 GHz $\gtrsim f \gtrsim$ 10 kHz, corresponding to a height range extending from the

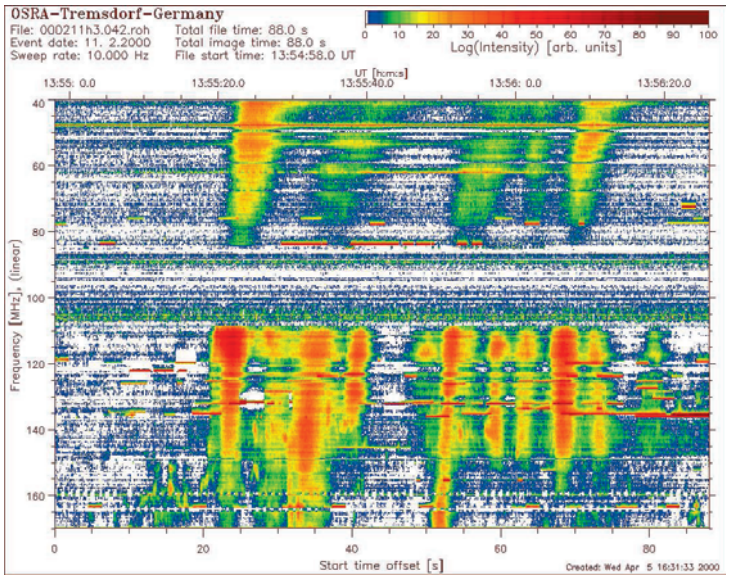

Figure 2.10: Group of type III bursts. OSRA. February 11, 2000. Adapted from http://www.aip.de/groups/osra/gal_2000/000211h3.gif.

low corona to beyond the orbit of the Earth. They were originally identified by their rapid drift ($df/dt \approx -0.01 f^{1.84}$, with f in MHz), short duration ($\Delta t \sim 220/f$, with f in MHz) and a relatively broad bandwidth at a given time due to their high drift rate. The bursts occur sporadically in isolation or in groups during a persistent storm. A significant fraction of type III bursts exhibit harmonic structure: the F and H components are seen simultaneously with their frequency ratio, from about 1:1.6 to 1:2.0. The fundamental emission is highly O mode polarized, and the second harmonic is weakly (15%) X mode polarized.

In general, bursts have low degrees of circular polarization, *i.e.* < 0.15. However, some bursts, those identified as fundamentals, have degrees of polarization up to about 0.5.

There are various subclasses of type III bursts. Inverted-U bursts turn over at some minimum frequency and then drift back from lower to higher frequency (Figure 2.11). J bursts are similar to U bursts without returning stroke. About 10% of the F components of type III bursts are type IIIb bursts, which consist of stria bursts (fine structures with double or triple splitting drifting more slowly than type III bursts), with an envelope similar to the profile of a type III burst.

Type III bursts are characteristic of the impulsive phase of solar flares: groups of several to several tens of type III bursts are associated with small to moderate-sized flares. There are also non-flare associated storm type III bursts.

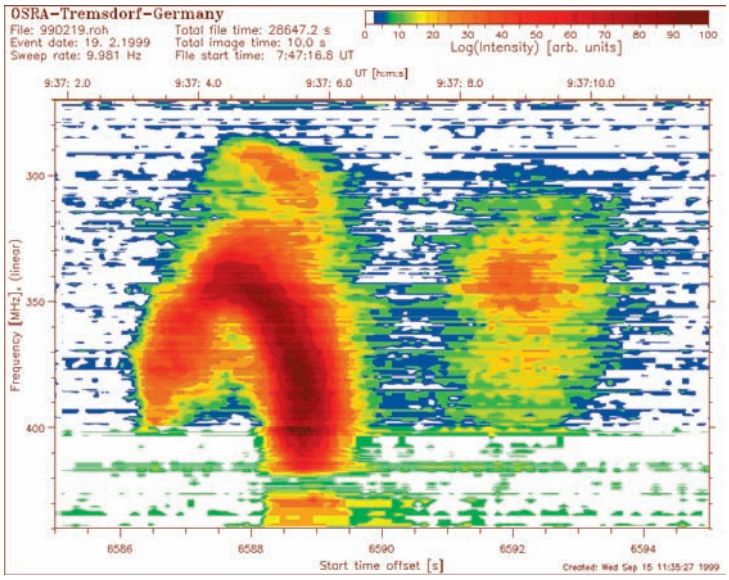

Figure 2.11: U burst. OSRA. February 19, 1999. Adapted from http://www.aip.de/groups/osra/gallery/990219.gif.

Interpretation: The exciting agency for type III bursts is a beam of energetic electrons, with speed $0.1c \lesssim v \lesssim 0.6c$, propagating outward from the Sun through the corona. These beams provide energy for the plasma emission mechanism. Inverted-U and J bursts are generally interpreted as being produced by electron beams traveling along closed magnetic field lines.

Stationary type IV bursts

Characteristics: A stationary type IV burst is a storm which follows a major flare. Initially the continuum is often intense with a few bursts, but it later evolves into a normal type I storm without any shift in the source position. During the early stages of an event the degree of circular polarization usually increases from a very low level to close to 100%.

Interpretation: The onset at a particular frequency indicates the arrival at the corresponding plasma level of a slowly expanding energy-release region in which the type I emission process takes place.

Moving type IV bursts (IVM)

Characteristics: A moving continuum source, which may be followed out from the Sun to large distances, but usually fades after moving up to $\sim 1R_{\odot}$ (Figure 2.12). Source speeds are roughly constant during any one event but range from 200 up to 1600 km $s^{-}1$. Most IVM bursts are observed for $\sim$ 30 min at 80 MHz, but some last as long as 2 hours.

Interpretation: The source is identified with a moving plasmoid ejected during a flare. Moving type IV radiation must be either: (a) gyro-synchrotron

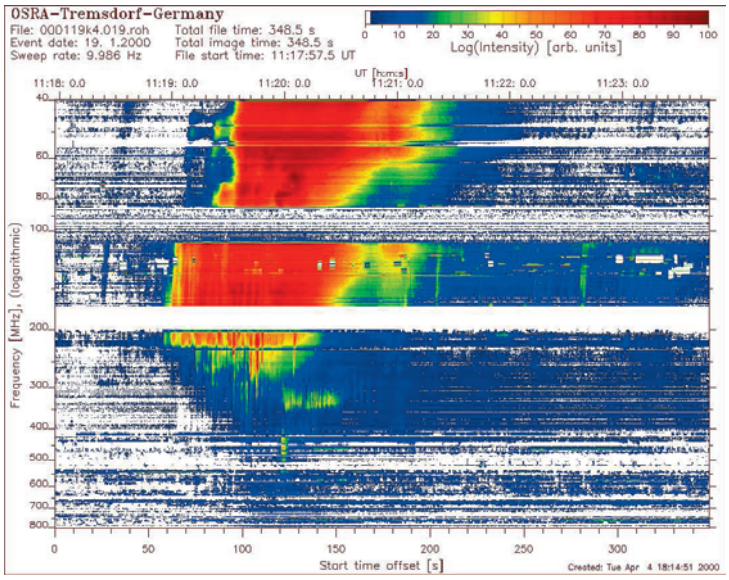

Figure 2.12: Type IV burst. OSRA. January 19, 2000. Adapted from http://www.aip.de/groups/osra/gal_2000/000119k4.gif.

emission from electrons with energy $\sim$ 100 keV in a strong magnetic field transported by the plasmoid; or (b) plasma emission. For plasma emission a the observed source heights the electron density in the plasmoid must be many times the normal background density. The gyro-synchrotron emission mechanism was accepted for many years and has been worked out in some detail. However, recent combined white light and radio observations support the plasma emission theory.

Type V bursts

Characteristics: A type V burst is a continuum burst which starts during shortly after a group of type III bursts and lasts for $\sim$ 2 min. The emission is particularly strong and long-lasting at frequencies between about 20 and 100 MHz. The degree of circular polarization is generally low, but when it is measurable the sense of polarization is usually opposite to that of the preceding type III bursts.

Interpretation: Early theories invoked synchrotron, or plasma emission from electrons trapped in high loops, but these have been rejected. Probably the best explanation for the long duration of type V bursts is that pitch-angle scattering removes electrons from the type III stream and slows down their propagation. The observed reversal of the sense of polarization between type III burst and the associated type V burst can be explained if the latter is due to the plasma emission from the scattered electrons.

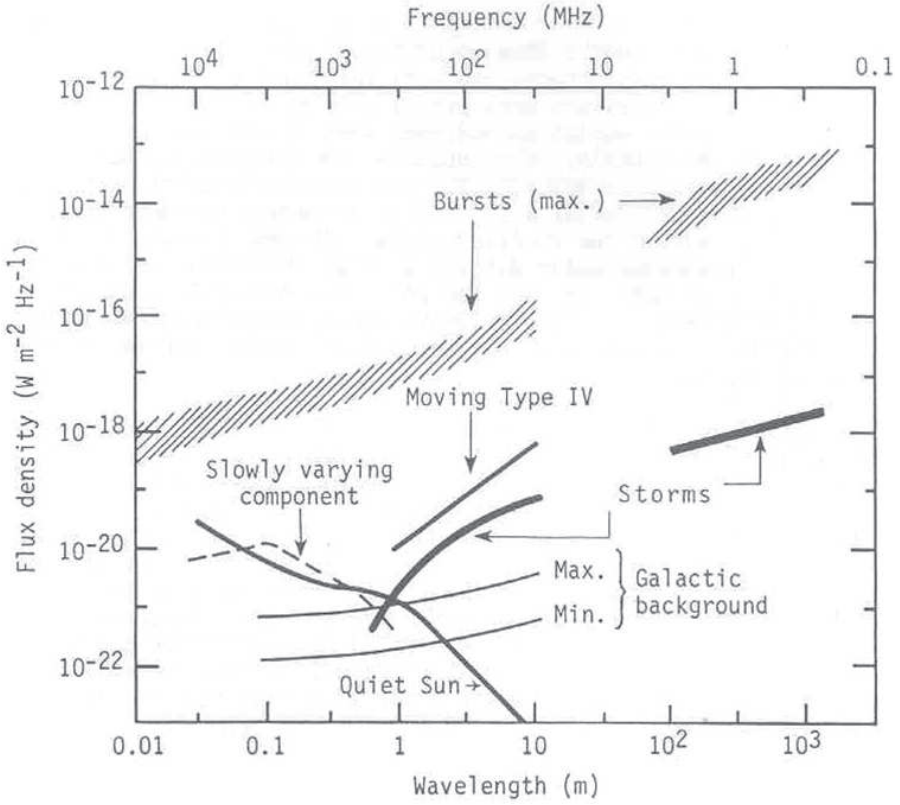

Figure 2.13: The overall background flux of the galactic background and the Sun at various activity levels [21].

2.3.3 Solar and galactic background flux density

Solar radio bursts are observed along with the background radiation coming from the Sun and our Galaxy. Let us briefly discuss the flux density levels of this radio sources. Figure 2.13 shows this for various states of solar activity as a function of frequency (scale along the top of the figure) and as a function of wavelength (scale along the bottom). The gap between about 2 MHz and 10 MHz is due to the ionosphere, which does not allow penetration of radio waves with the frequency below the maximum plasma frequency in the ionosphere (about 10 MHz), and observations from space at the time of this figure were limited to the maximum frequency of about 2 MHz. Nowadays, spacecraft measurements have closed the gap (going up to 15 MHz with the WIND spacecraft), and the curves shown with gaps actually join together rather continuously. At quiet times, the Sun dominates down to about 300 MHz, but below that the galactic background dominates. The curve labeled slowly varying component basically means active regions, which may slightly dominate the quiet Sun in flux density, but rather strongly dominate in terms of brightness temperature. At times of storm activity and outbursts, the Sun can dominate

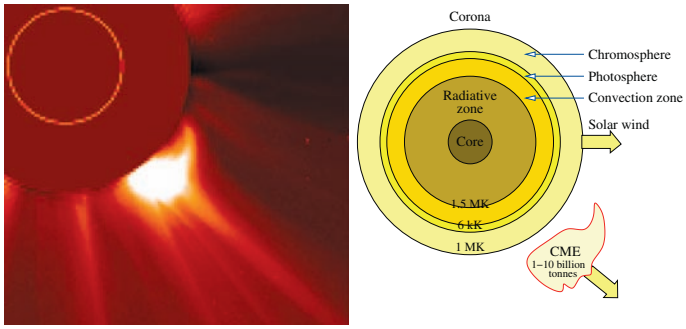

Figure 2.14: Coronal mass ejections (CMEs) have been identified in the optical frequency range by instruments as LASCO on the *SOHO* spacecraft (left) [52].

strongly at all frequencies, being four or five orders of magnitude above the quiescent Sun at lower frequencies.

2.4 Coronal mass ejections (CMEs)

Coronal mass ejections (CMEs) constitute a form of intermittent massive expulsion of mass from the solar corona (Figure 2.14). They may appear with a frequency of one event per every few days during solar minimum to several events per day during solar maximum. They form a bursty type of solar activity and are—if earthward directed—known to be a key causal link between solar events and geomagnetic storms [37, 44].

CMEs were first directly identified in white-light images from a coronagraph flown on *OSO-7* [88] and their rather frequent occurrence has been established through continuous space-borne observations on *OSO-7* [88], *Skylab* [54] and various subsequent spacecraft. The Large Angle and Spectrometric Coronagraph Experiment (LASCO) [9] flown on the *Solar Heliospheric Observatory (SOHO)* [15], launched in 1995, has by now provided the most extensive set of CME observations at different optical and near-optical wavelengths during solar conditions ranging from solar minimum to solar maximum. Optical signatures of CME structures have been observed from 1.1 out to 30 solar radii (the inner and outer limits of the LASCO field-of-view).

Only 65% of the shocks observed as fast ($v > 500$ km s^{-1}) coronal mass ejection radiate type II emission [6]. On the other hand, CMEs slower than 200 km s^{-1} are occasionally accompanied by type II bursts [43].

At solar minimum, the vast majority of CMEs is produced at low solar latitudes, and at solar maximum, at virtually all latitudes in a regime of slow to moderate ambient solar wind speed. At the inner edge of the coronagraph images, CMEs are observed to start at a wide range of velocities, often at a rather low speed of a few tens of km/s, and then they frequently undergo

acceleration all the way to the outer edge of the coronagraph image [39] up to a velocity of many hundreds of km/s.

The typical CME structure (33% of the cases according to [10]) can be related to the well-known prominence-cavity pattern leading to a three-part configuration: a leading density enhancement, followed by a density depletion, the disconnected coil-shaped flux system supporting the former prominence, again followed by another density enhancement part of the uplifting prominence. The probable conservation of the magnetic support of the former prominence is the physical key factor for the later identification of in-situ observed magnetic clouds in the solar wind with preexisting CMEs and before existing prominences on the disc.

The other extreme of the CME morphology is a diffuse and structure-less mass cloud (about 25% of the cases). The total mass ejected in one single CME is typically in the 10^{12} to 10^{13} kg range [36]. The plasma temperature and density within CMEs seem to be highly inhomogeneous. There exist early reports on long-standing confinement of cold prominence matter within the CME body. Woo [93] presents a density and density inhomogeneity histogram of different coronal structure elements including CMEs.

At large distances from the Sun, the plasma density and plasma speed in CMEs are not necessarily different from those of the ambient solar wind. A number of characteristic features including low ion and electron temperatures, counter-streaming suprathermal electrons and energetic ions, higher alpha particle abundance and a strong magnetic field are often found to be associated with CMEs [70].

From solar observations it is evident that the explosive, short time-scale energy release during flares and the long term, gradual energy release expressed by CMEs can be reasonably understood only if both processes are taken as common and probably not independent signatures of a destabilisation of preexisting coronal magnetic field structures. Configurations of several active regions, quiescent prominences and large scale magnetic arcades outside active regions can be source regions of CME formation. The study of formation, acceleration, and propagation of CMEs requires advanced and powerful observational tools in different spectral ranges at as many “levels” as possible between the photosphere of the Sun and the magnetosphere of the Earth.

2.5 Transition radiation

In Paper IV we present *in situ* satellite observation of the source of radio emission of associated with a CME-driven interplanetary shock. The intense emissions above the electron plasma frequency along with the energetic particles are observed in close vicinity of the ramp of the shock. We suggest that the generation takes place locally at the shock front and just behind it and propose a generation mechanism known in electrodynamics as transition radiation.

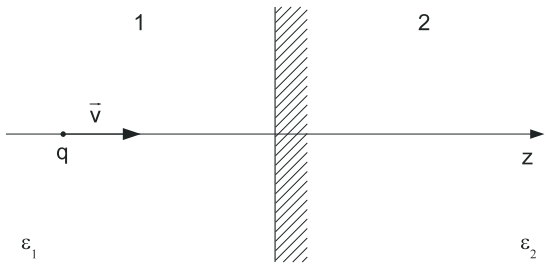

Figure 2.15: Crossing a boundary of two media by a charge q.

The process of transition radiation is a very general one. It appears if some source, which does not have a proper frequency (for example a point charge, multipole etc.), is moving with a constant velocity in an inhomogeneous and/or nonstationary medium. Here we present the theory of transition radiation by the simplest example of the crossing by a charge the boundary of two media [25, 26]. In this case the most simplest explanation of the transition radiation is as follows. It is well known that the electromagnetic field of the charge in one (the first) of the two media can be constructed as a superposition of the field of the charge "itself" and the field of an "image" charge, which moves in the other (second) medium. At the moment when the charge is on the boundary from the "point of view" of the field in the first medium the charge and its "image" partially "annihilate" each other, which creates radiation.

Transition radiation on a boundary of two media

1. Initial equations. Let us consider first the main and the simplest (in some sense) problem of the theory of transition radiation, appearing when a charge q with a constant velocity v passes through a boundary of two media [17]. For simplicity, we will suppose that the charge is moving in the direction normal to the boundary (see Figure 2.15). The isotropic media 1 and 2 are characterized by the dielectric permittivities ε_1, and ε_2, which have in a general case complex values. The starting equations are obviously the equations for the fields

$$\nabla \times \mathbf{B} = \frac{1}{c}\frac{\partial \varepsilon \mathbf{E}}{\partial t} + \frac{4\pi}{c}\mathbf{j}^q; \quad \nabla \times \mathbf{E} = -\frac{1}{c}\frac{\partial \mathbf{B}}{\partial t}, \tag{2.5}$$

for which the current density of a charge q has the form

$$\mathbf{j}^q = q\mathbf{v}\delta(r - \mathbf{v}t). \tag{2.6}$$

Since the problem is homogeneous in time and homogeneous in both of the media in the directions perpendicular to the particle trajectory, it is useful to decompose all the quantities (fields, current, density etc.) in Fourier components in time and in the coordinates $\mathbf{r}_\perp$ perpendicular to the charge trajectory

(the z axis perpendicular to the boundary). Then

$$\begin{aligned} j_z^q(\mathbf{r},t) &= \int j^q_{\boldsymbol{\kappa},\omega}(z)\, e^{i\boldsymbol{\kappa}\mathbf{r}_\perp - i\omega t}\, d\boldsymbol{\kappa}\, d\omega, \\ \mathbf{E}(\mathbf{r},t) &= \int \mathbf{E}_{\boldsymbol{\kappa},\omega}(z)\, e^{i\boldsymbol{\kappa}\mathbf{r}_\perp - i\omega t}\, d\boldsymbol{\kappa}\, d\omega, \qquad (2.7) \\ \mathbf{B}(\mathbf{r},t) &= \int \mathbf{B}_{\boldsymbol{\kappa},\omega}(z)\, e^{i\boldsymbol{\kappa}\mathbf{r}_\perp - i\omega t}\, d\boldsymbol{\kappa}\, d\omega. \end{aligned}$$

(2.8)

Here vector $\boldsymbol{\kappa}$ has two components κ_x and κ_y. For the component j_z^q of the current density $\mathbf{j}^q$ we find from (2.6)

$$j^q_{\boldsymbol{\kappa},\omega}(z) = \frac{q}{(2\pi)^3}\, \exp\frac{i\omega z}{v}. \qquad (2.9)$$

2. The field, created by the charge crossing the boundary of two media. It is useful to divide the total $\mathbf{E}$ into the component along the charge trajectory, denoted simply by E, and a perpendicular component $\mathbf{E}_\perp$. By the definitions

$$E = \frac{1}{v}(\mathbf{E}\cdot\mathbf{v}); \quad \mathbf{E}_\perp = \mathbf{E} - \frac{1}{v^2}\mathbf{v}(\mathbf{E}\cdot\mathbf{v}). \qquad (2.10)$$

The vector $\mathbf{E}_\perp$ has two components E_x and E_y. Below we will mainly use the field equation in the Fourier decomposition (2.7) and, therefore, for simplicity, we will not keep the indices $\boldsymbol{\kappa}$ and ω for the corresponding Fourier components. We think this will not lead to confusion. We can find for these components, by a projection of equations (2.5) on the direction of the charge velocity $\mathbf{v}$, the following equation

$$\kappa_x B_y - \kappa_y B_x = -\frac{\omega}{c}\varepsilon E - \frac{4\pi i}{c} j^q, \qquad (2.11)$$

$$B_y = -\frac{c}{\omega}\left(\kappa_x E + i\frac{\partial E_x}{\partial z}\right); \quad B_x = \frac{c}{\omega}\left(\kappa_y E + i\frac{\partial E_y}{\partial z}\right). \qquad (2.12)$$

From these equations it follows that

$$\left(\kappa^2 - \frac{\omega^2}{c^2}\varepsilon\right) E + i\frac{\partial}{\partial z}(\boldsymbol{\kappa}\mathbf{E}_\perp) = \frac{4\pi i\omega q}{c^2(2\pi)^3}\, \exp\frac{i\omega z}{v}, \qquad (2.13)$$

where $\kappa^2 = \kappa_x^2 + \kappa_y^2$. The charge current does not contribute to the projection of the Maxwell equations on the direction perpendicular to the charge velocity, and we find

$$\left(\frac{\partial^2}{\partial z^2} + \frac{\omega^2}{c^2}\varepsilon\right)(\boldsymbol{\kappa}\mathbf{E}_\perp) = i\kappa^2\frac{\partial E}{\partial z}. \qquad (2.14)$$

We can eliminate $\boldsymbol{\kappa}\mathbf{E}_\perp$ from these equations by applying the operator $\partial^2/\partial z^2 + (\omega^2/c^2)\varepsilon$ to both sides of equation (2.13) and by using (2.14). This gives a single equation for E:

$$\frac{\partial^2}{\partial z^2}\varepsilon E + \varepsilon\left(\frac{\omega^2}{c^2}\varepsilon - \kappa^2\right) E = -\frac{4\pi i\omega q}{c^2(2\pi)^3}\left(\varepsilon - \frac{c^2}{v^2}\right)\, \exp\frac{i\omega z}{v}. \qquad (2.15)$$

In derivation of (2.15) we took into account that inside each of the media 1 and 2 the dielectric permittivity ε is constant and does not depend on z. But on the boundary ε has a jump. Equation (2.15) can be solved in each medium and the solutions should be joined by using the boundary conditions which are nothing but an equality on the boundary of the normal components of the inductions and tangential components of the electric fields [1]

$$\varepsilon_1 E_1|_{z=0} = \varepsilon_2 E_2|_{z=0}; \quad (\boldsymbol{\kappa}\mathbf{E}_\perp)_1|_{z=0} = (\boldsymbol{\kappa}\mathbf{E}_\perp)_2|_{z=0}. \tag{2.16}$$

Let us consider first the solution of (2.15) for a homogeneous medium (which could be one of the two media). Such a solution will be a sum of a field induced by the charge (the charge field in the medium)

$$E^q = -\frac{4\pi i q(1-c^2/v^2\varepsilon)}{\omega(2\pi)^3(\varepsilon - c^2/v^2 - \kappa^2 c^2/\omega^2)} \exp\frac{i\omega z}{v} \tag{2.17}$$

and the free field (the field of the emitted radiation)

$$E^R = -\frac{4\pi i q}{\omega(2\pi)^3} a \exp\left\{\mp i\frac{\omega}{c}\sqrt{\varepsilon - \frac{\kappa^2 c^2}{\omega^2}}z\right\}. \tag{2.18}$$

Remember that $E = E^q + E^R$ is a component of $\mathbf{E}$ along the charge velocity $\mathbf{v}$. The factor $4\pi i q/\omega(2\pi)^3$ in the amplitude of the radiation field was introduced only for simplification of the further calculations. The amplitude a then becomes dimensionless. The "+" sign in (2.18) corresponds to a wave propagating in the $z > 0$ direction and a "–" sign corresponds to the wave propagating in the $z < 0$ direction. The field E^R in the wave zone will be the field of the transition radiation. This field should propagate from the boundary, i.e. in medium 2 it is necessary to use the "+" sign in (2.18) and in medium it is necessary to use the "–" sign in (2.18).

It is necessary to mention two reservations. Strictly speaking, the field (2.18) is a radiation field only in the case when (2.18) describes a propagating wave, *i.e.* when

$$\varepsilon > \kappa^2 c^2/\omega^2. \tag{2.19}$$

For $\varepsilon < \kappa^2 c^2/\omega^2$ the field (2.18) should decrease exponentially from the boundary. This means that for both the "+" and "–" signs it is necessary to use for (2.19) the relation

$$\sqrt{\varepsilon - \frac{\kappa^2 c^2}{\omega^2}} = i\frac{\omega}{|\omega|}\sqrt{\frac{\kappa^2 c^2}{\omega^2} - \varepsilon}. \tag{2.20}$$

Such fields decreasing from the boundary should without doubt be present in the consideration of transition radiation since the waves excited by the charge

[1] Here and further the lower indices 1, 2 correspond to the field in the medium 1 and medium 2, respectively; for the signs $\pm$ and $\mp$ the upper sign corresponds to the medium 1, and the lower to the medium 2.

can afterwards be completely reflected by the boundary. Strictly speaking, there exists also a transition radiation of the surface waves. This process is not considered here.

The second reservation concerns the possibility of existence of a solution of the homogeneous equation (2.15) $\varepsilon = 0$, which corresponds to emission of longitudinal waves. The characteristics of these waves depend very essentially on the spatial dispersion and consequently on the properties of the medium close to the boundary. We will not consider them here either.

Considering the transition radiation we will suppose that the criteria for Vavilov-Cherenkov emission are not fulfilled (*i.e.* we suppose that $c^2/v^2\varepsilon > 1$). To use the boundary conditions (2.16) it is necessary to know the tangential components of the electric fields. They can be easily found from (2.14) for the charge field (index q) and for the radiation field (index R)

$$(\boldsymbol{\kappa}\mathbf{E}_\perp)^q = -\frac{\kappa^2 c^2}{v\omega(\varepsilon - c^2/v^2)}E^q; \quad (\kappa\mathbf{E}_\perp)^R = \pm\frac{\omega}{c}\sqrt{\varepsilon - \frac{\kappa^2 c^2}{\omega^2}}E^R. \tag{2.21}$$

It is possible then to use the boundary conditions (2.16) to find two equations for the two amplitudes a_1, and a_2 of the radiation fields in media 1 and 2

$$\frac{\kappa^2 c^2/\omega^2}{\varepsilon_1 - c^2/v^2 - \kappa^2 c^2/\omega^2} - \varepsilon_1 a_1 = \frac{\kappa^2 c^2/\omega^2}{\varepsilon_2 - c^2/v^2 - \kappa^2 c^2/\omega^2} - \varepsilon_2 a_2, \tag{2.22}$$

$$\begin{aligned}\frac{\kappa^2 c^2/\omega^2}{v\varepsilon_1(\varepsilon_1 - c^2/v^2 - \kappa^2 c^2/\omega^2)} + \frac{1}{c}\sqrt{\varepsilon_1 - \frac{\kappa^2 c^2}{\omega^2}}a_1 = \\ \frac{\kappa^2 c^2/\omega^2}{v\varepsilon_2(\varepsilon_2 - c^2/v^2 - \kappa^2 c^2/\omega^2)} - \frac{1}{c}\sqrt{\varepsilon_2 - \frac{\kappa^2 c^2}{\omega^2}}a_2.\end{aligned} \tag{2.23}$$

It is not at all difficult to solve this system of equations with respect to the amplitudes a_1, and a_2:

$$\begin{aligned}a_2 = \quad & \frac{v}{c}\frac{\kappa^2 c^2}{\omega^2}\frac{1}{\varepsilon_1\sqrt{\varepsilon_2 - \kappa^2 c^2/\omega^2} + \varepsilon_2\sqrt{\varepsilon_1 - \kappa^2 c^2/\omega^2}} \times \\ & \left(\frac{1 + \frac{v}{c}\sqrt{\varepsilon_1 - \frac{\kappa^2 c^2}{\omega^2}}}{1 - \frac{v^2}{c^2}\varepsilon_1 + \frac{\kappa^2 v^2}{\omega^2}} - \frac{\frac{\varepsilon_1}{\varepsilon_2} + \frac{v}{c}\sqrt{\varepsilon_1 - \frac{\kappa^2 c^2}{\omega^2}}}{1 - \frac{v^2}{c^2}\varepsilon_2 + \frac{\kappa^2 v^2}{\omega^2}}\right),\end{aligned} \tag{2.24}$$

$$\begin{aligned}a_1 = \quad & -\frac{v}{c}\frac{\kappa^2 c^2}{\omega^2}\frac{1}{\varepsilon_1\sqrt{\varepsilon_2 - \kappa^2 c^2/\omega^2} + \varepsilon_2\sqrt{\varepsilon_1 - \kappa^2 c^2/\omega^2}} \times \\ & \left(\frac{1 - \frac{v}{c}\sqrt{\varepsilon_2 - \frac{\kappa^2 c^2}{\omega^2}}}{1 - \frac{v^2}{c^2}\varepsilon_2 + \frac{\kappa^2 v^2}{\omega^2}} - \frac{\frac{\varepsilon_2}{\varepsilon_1} - \frac{v}{c}\sqrt{\varepsilon_2 - \frac{\kappa^2 c^2}{\omega^2}}}{1 - \frac{v^2}{c^2}\varepsilon_1 + \frac{\kappa^2 v^2}{\omega^2}}\right).\end{aligned} \tag{2.25}$$

It is easy to see that a_1 can be obtained from a_2 by substituting $\varepsilon_1 \rightleftarrows \varepsilon_2$ and $v \to -v$.

3. The energy of transition radiation. Let us find an expression for the energy of the emitted transition radiation in terms of the amplitudes a_1, and a_2. To find this value it is not necessary to calculate the Poynting vector, but it is sufficient to calculate the energy of the radiation field E^R asymptotically as $t \to \infty$, when the radiation field and the charge field are separated. We will also suppose that the medium in which we consider the transition radiation to be transparent. This method of calculating the energy emitted corresponds to the Hamiltonian method described in [24]. For simplicity we will neglect the dispersion of dielectric permittivity in our calculations of the energy emitted and will take into account that for electromagnetic wave the electric and the magnetic energies are equal

$$W_2^R = \frac{1}{4\pi} \int d\mathbf{r}_\perp \int_0^\infty dz\, \varepsilon_2 \left[(E^R)^2 + (E_\perp^R)^2 \right]. \tag{2.26}$$

Index 2 shows that the radiation in medium 2 (*i.e.* in a forward direction) is considered. The result obtained (although the dispersion of ε_2 was neglected in the derivation of the result) is valid for any dispersive medium. The factor $\frac{1}{2}\partial/\partial\omega(\omega^2\varepsilon_2(\omega))$ which replaces the factor ε_2 in (2.26) in the case of dispersing media is canceled as can be seen from the calculations given below. Let us insert the decomposition (2.7) into (2.26) and take into account that according to (2.20) we have

$$|\mathbf{E}_\perp^R|^2 = (\omega/\kappa^2 c^2)(\varepsilon_2 - \kappa^2 c^2/\omega^2)|E^R|^2. \tag{2.27}$$

Then we obtain

$$\begin{aligned} W_2^R &= \pi^2 \lim_{t\to\infty} \int_0^\infty \int_{-\infty}^\infty d\omega\, d\omega'\, |E^R|^2 \times \\ &\qquad \frac{\omega^2 \varepsilon_2^2 \sin\left[(\omega-\omega')t\right]}{\kappa^2 c^2 \left[(\omega/c)\sqrt{\varepsilon_2 - \kappa^2 c^2/\omega^2} - (\omega'/c)\sqrt{\varepsilon_2 - \kappa^2 c^2/\omega'^2} \right]} \end{aligned} \tag{2.28}$$

We can find finally by using the relation

$$\lim_{t\to\infty} \frac{1}{\pi} \frac{\sin\left[(\omega-\omega')t\right]}{\omega-\omega'} = \delta(\omega-\omega'), \tag{2.29}$$

that

$$\begin{aligned} W_2^R &= 2\pi^3 \int_0^\infty \frac{\omega^2}{\kappa^2 c^2} \varepsilon_2 \sqrt{\varepsilon_2 - \frac{\kappa^2 c^2}{\omega^2}} |E^R|^2 d\boldsymbol{\kappa}\, d\omega \\ &= \frac{q}{2\pi c} \int_0^\infty \frac{d\kappa^2}{\kappa^2} |a_2|^2 \varepsilon_2 \sqrt{\varepsilon_2 - \frac{\kappa^2 c^2}{\omega^2}}\, d\omega \end{aligned} \tag{2.30}$$

It is useful to introduce the angle θ_2 between $\mathbf{k}$ and $\mathbf{v}$ (remember that the charge moves normally to the boundary from medium 1 to medium 2). Then

$$\sin^2\theta_2 = \kappa^2 c^2/\omega^2\varepsilon_2.$$

We find the total energy emitted into medium 2 (i.e. in a forward direction) by taking into account relation (2.25)

$$W_2^R = \int_0^\infty d\omega \int_0^{\pi/2} 2\pi W_2^R(\omega,\theta_2)\, 2\pi \sin\theta_2\, d\theta_2, \tag{2.31}$$

where

$$W_2^R(\omega,\theta_2) = \frac{q^2v^2\sqrt{\varepsilon_2}\,|\varepsilon_2-\varepsilon_1|^2\sin^2\theta_2\cos^2\theta_2}{\pi^2c^3|\varepsilon_1\cos\theta_2+\sqrt{\varepsilon_2}\,\sqrt{\varepsilon_1-\varepsilon_2\sin^2\theta_2}|^2}\times$$
$$\times\frac{\left|1-\dfrac{v}{c}\sqrt{\varepsilon_1-\varepsilon_2\sin^2\theta_2}-\dfrac{v^2}{c^2}\varepsilon_2\right|^2}{\left|\left(1-\dfrac{v^2}{c^2}\varepsilon_2\cos^2\theta_2\right)\left(1-\dfrac{v}{c}\sqrt{\varepsilon_1-\varepsilon_2\sin^2\theta_2}\right)\right|^2}. \tag{2.32}$$

The radiation emitted into medium 1 W_1^R (i.e. in a backward direction) can be obtained from W_1^R by swapping $\varepsilon_1 \rightleftarrows \varepsilon_2$, $v \to -v$, and $\theta_2 \to \theta_1$, where θ_1 is the angle between $\mathbf{k}$ and $-\mathbf{v}$.

3. Solar radar experiments

In this chapter we review solar radar experiments. It is based essentially on review by *Gordon* [34], which is revised and complemented.

3.1 A review of solar radar experiments

The first solar radar experiment was conducted in 1959 at a frequency of 25.6 MHz [18]. Transmitters with comparatively low power (≈40 kW) and also the inadequate gain of the broad side array (≈25 dB) over the isotropic radiator, could only demonstrate that solar echos were actually detected during a successful three-day experiment. On the grounds of the reduction of the data carried out later on with allowance for the frequency spreading of the reflected signal, an estimation of the scattering cross-section was performed. The estimated value ($\sigma \approx 80\ \pi {R_\odot}^2$) [17] was found to be much higher than that expected from theoretical considerations. Repeated attempts to obtain radio echoes at the same frequency, undertaken in the years 1963, 1964 and 1965 (the total number of experiments exceeded 200) failed to detect any significant signal although the transmitters' power was raised to 300 kW [72]. As a result of these experiments only the upper limit of the cross-section ($\approx 2\ \pi {R_\odot}^2$) could be estimated.

An attempt was also made to obtain radio echos at 450 MHz with the aid of the 1000-ft radio telescope in Arecibo but it was also unsuccessful [16]. Radar experiments at 50 MHz were carried out also by Bowles at the radar observatory in Jicamarca (Peru). For several series of experiments, in which the combination of the transmitters output power and the gain of the antenna array was more favourable than in all known solar radar experiments, the results were negative [16].

Systematic radar studies of the Sun began in 1961 at the Lincoln Laboratory of the Massachusetts Institute of Technology radar station near El Campo, Texas [41]. The antenna was constructed in the form of an array of 1016 half-wave dipoles distributed on an area of 9 acres (Figure 3.1). A fan-beam aperture with EW dimensions equal to 6.5° and NS dimension of 0.7°, allowed the observation of the radio echo from the Sun during its culmination. The transmission of the coded signal lasted for 16 minutes – the round trip time of the signal travel, and thereupon the reception of the radio echo began.

The gain for the zenith direction equaled 36 dB above that of an isotropic radiator. The power supply by the transmitter to the antenna in the continu-

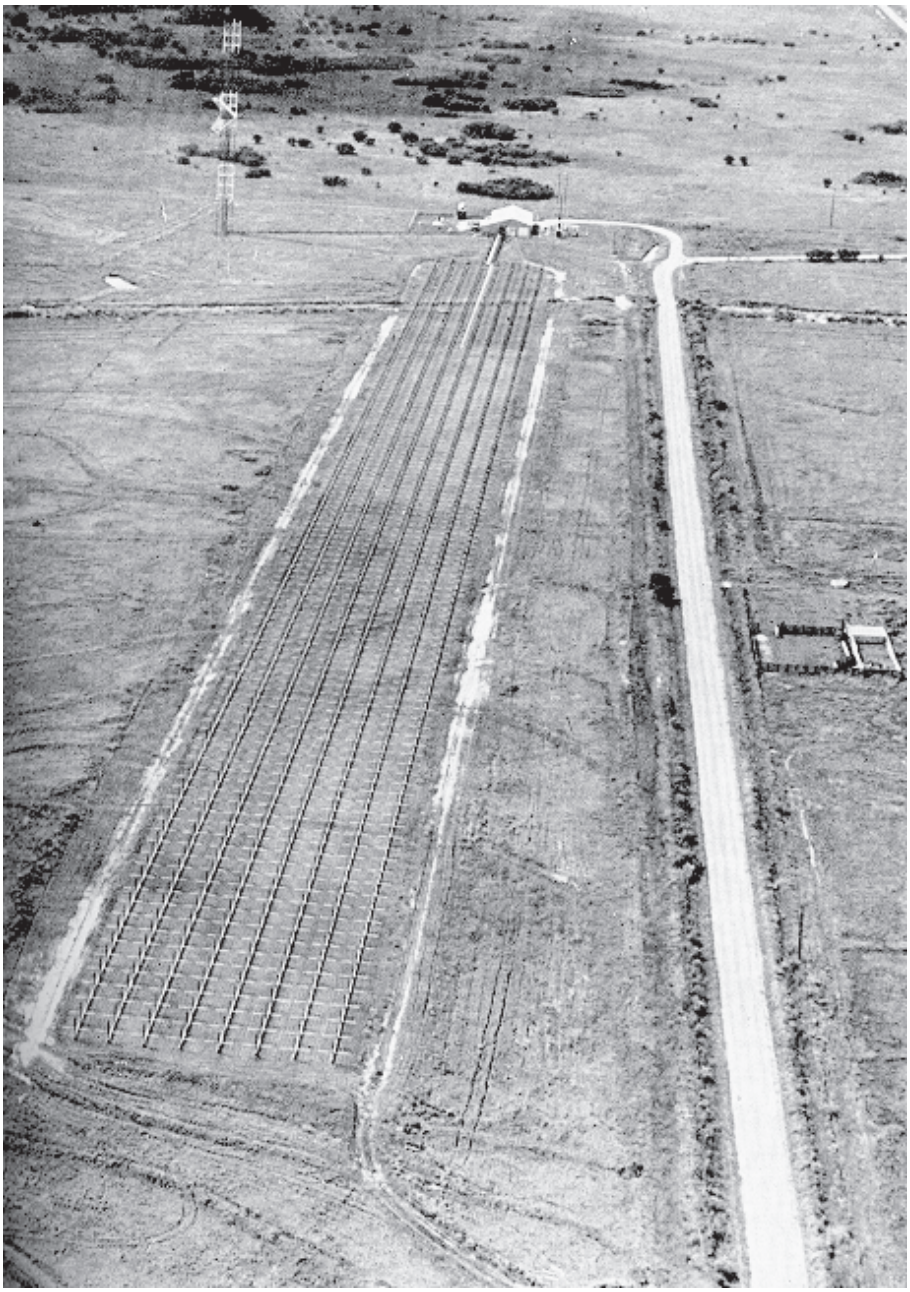

Figure 3.1: El Campo solar radar.

ous wave signal regime was between 480 and 500 kW. As the received signal was 20 to 30 dB lower than the noise level, an integration time of $\approx 10^3$ sec was usually needed. The contribution of the galactic radiation and of sporadic radio-emission of the Sun was eliminated by subtracting the outputs obtained in two frequency ranges — the first range containing the radio echo components, and the second, being free from the echo components. For about 5 to 10% of the daily experiments, the echo energy was insufficient to obtain reliable values of the cross-section. The limit of detectability was $\approx 0.1\ \pi {R_\odot}^2$. For about 75% of the experiments the energy received was insufficient to obtain significant frequency shift-time delay spectra. All the spectra which have appeared in different publications correspond to cross-sections between limits from about 1 $\pi {R_\odot}^2$ to about 7 $\pi {R_\odot}^2$. The spectra corresponding to larger cross-sections are absent, probably because of a high level of interferences. Spectra corresponding to smaller cross-sections are difficult to obtain because of the low signal-to-noise ratio (SNR).

Along with the individual spectra the number of average spectra corresponding to a definite period of time or selected by large or small scattering cross-sections, by the presence of components reflected from high levels in the corona, were also published.

In 44 cases out of a total of 1144 experiments presented in the report by James [42], reflections from the back-side of the Sun were detected. In 17 cases cross-section was smaller than 2 $\pi {R_\odot}^2$ and sometimes as high as 30 $\pi {R_\odot}^2$ were recorded. But no ideas about the interpretation of these apparently quite reliable observations were offered.

In 1977 and 1978 Benz and Fitze attempted to observe scatter from Langmuir waves in the corona using a 2380 MHz, 500 MW CW transmitter at Arecibo [7, 20] but were not successful, most likely because of the very high frequency used.

From 1996 to 1998 solar radar experiments were carried out at 9 MHz using the Russian Sura high-power radio transmitter together with the Ukrainian UTR-2 radio telescope in a bistatic mode [79, 77], and there was a likely marginal detection of the corona with a Doppler bandwidth of about 40 kHz. During this period Sura was also used in a monostatic mode at 9 MHz [46, 47]; the analysis of the monostatic data is still in progress [45].

3.2 Main results of El Campo experiments

3.2.1 Scattering cross-sections

In spite of the theoretical prediction of the scattering cross-section of the Sun at 38.25 MHz to be $\approx 1.5\ \pi {R_\odot}^2$ (see Section 4.3) the experiment shows variation of the scattering cross-sections within very wide limits, over four orders of magnitude, ranging from $\approx 800\ \pi {R_\odot}^2$ to $\approx 0.1\ \pi {R_\odot}^2$ and lower [42]. As

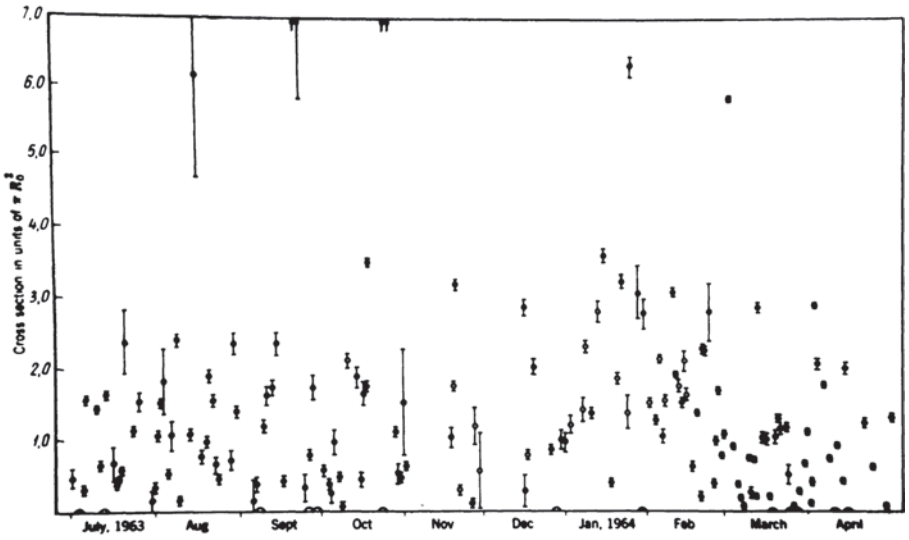

Figure 3.2: Scattering cross-sections observed by James [42]. Corrections allowing for the band width are introduced according to James [42]

to the character of these changes, see Figure 3.2. It must be emphasized that possible changes of the global electron density and the temperature of corona can neither explain the very large nor the very small cross-sections observed at El Campo.

A comparison of the large cross-sections observed with the angular aperture of the beam of the receiving antenna makes it evident that the reflected signal must be highly directive or (and) significantly amplified during the two-way propagation in the corona. It will be shown below that the reflection takes place only above active regions. This makes the demand on the mechanisms of the directivity and (or) amplification even higher.

The second remarkable feature of these observations is the rapid day-to-day change of the cross-sections. There are, for instance, some cases when in two successive experiments the effective cross-section increased from $0.6\ \pi {R_\odot}^2$ to $251\ \pi {R_\odot}^2$. In another case, in three consecutive days after the decrease of the cross-section from $151\ \pi {R_\odot}^2$ to $\sigma < 0.1\ \pi {R_\odot}^2$, a new rise to $\sigma = 185\ \pi {R_\odot}^2$ was observed. It is of vital importance for the elucidation of the mechanism which is responsible for the formation of the radio echo from the Sun that the increase in the effective cross-section is invariably accompanied by a rise in the level and an enhancement of the fluctuations of the Sun's sporadic radio emission at 38 MHz. It is interesting to note that these coincidences were of such a remarkable character that it permitted James to formulate the conclusion: "This suggests very strongly that the same mechanism was responsible for both the noise level and the increase in cross-section" [41].

3.2.2 Structure of radio echo spectra

A typical spectrum of a reflected signal in James' experiment is presented in Figure 3.3. The main part can be distinguished in this spectrum. Its component usually originates from layers with heliocentric distances in the direction of the observer $\approx (1.2-1.5)\ R_{\odot}$, and with a thickness of $\approx 0.3\ R_{\odot}$. Along with the main part of the spectrum, which contains the principal portion of the reflected energy, diffuse components can be observed at different distances and with different frequency shifts. These spectra were classified as spectra of type A [32]. Their fraction amounts to 70%.

There are also spectra in which the main part cannot be distinguished. Spectra of this kind are classified as type B spectra; they possess a more diffuse character, the reflected energy is more smoothly distributed between different ranges (see Figure 3.4). A predominant number of type A spectra is observed when there are plage areas near the center of the solar disk [32].

A remarkable feature of the time-frequency structure of radio echo spectra is the quasi-symmetric distribution of the frequency shifts in which the total energy contained in the positive and negative components is of the same order of magnitude. Such a structure is quite unexpected because in the model of the reflection from moving inhomogeneities frozen into the solar wind an overwhelming predominance of the "red" shifted components would be expected.

The second unexpected feature of the radio echo spectra is the persistent presence of components with high-frequency displacements up to 50 kHz and more. In the case of a Doppler nature of these frequency shifts the corresponding velocities components would be as high as 200 km/s and still higher. From the quasi-symmetric structure of the signal, a complete equality of the number of descending and ascending motions follows in self-evident contradiction to the theory of the solar wind.

The third peculiarity of the radio-echo data is the presence of components reflected from very high levels in the corona, up to 5.2 $R_{\odot}$, see Figure 3.5. In the model of the reflections from the layer with a refraction index $n = 0$ (specular reflection), an enhancement by three orders of magnitude of the undisturbed coronal density is required. Such a density enhancement cannot be reached in shock waves.

3.2.3 Comparison of the results of radar experiments with the characteristics of solar activity

A study by Gerasimova (1974) [22] was performed in order to find the correlation between the scattering cross-sections and the area of the hot radio emission region observed at 9.1 cm. The results are in accordance with those obtained by James [41], who found that no stable correlation between the cross-sections and plage areas exists. Autocorrelation curves were constructed

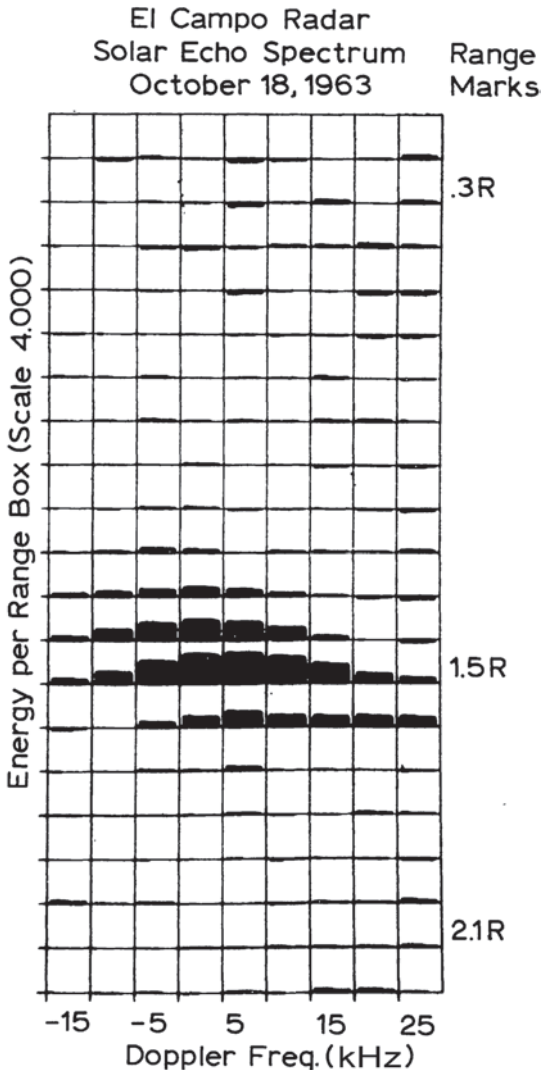

Figure 3.3: Radio echo spectrum [41] of type A, presenting the distribution of the received energy according to different ranges and frequency displacements. Range marks are located on the delay-time scale for an assumed excess group delay of two seconds.

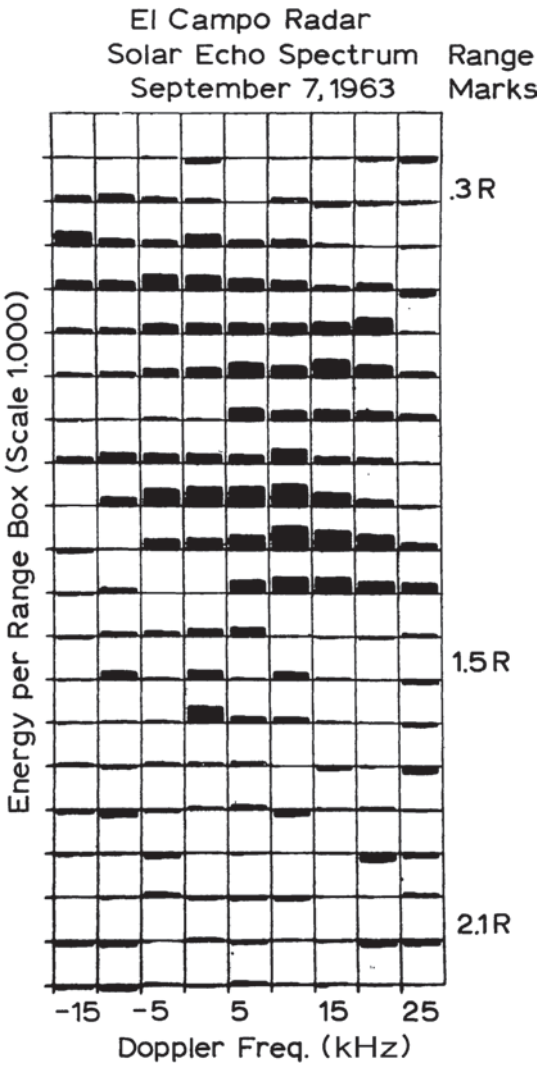

Figure 3.4: Radio echo spectrum [41] of type B. The distribution of energy between different delays and frequency shifts is more diffuse than in the spectra of type A.

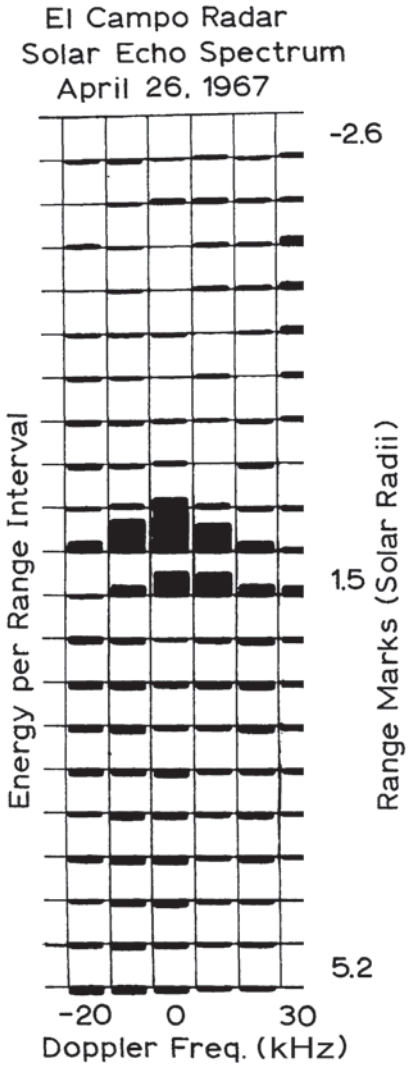

Figure 3.5: Radio echo spectra are characterized by the presence of components reflected from very high layers of the corona [42].

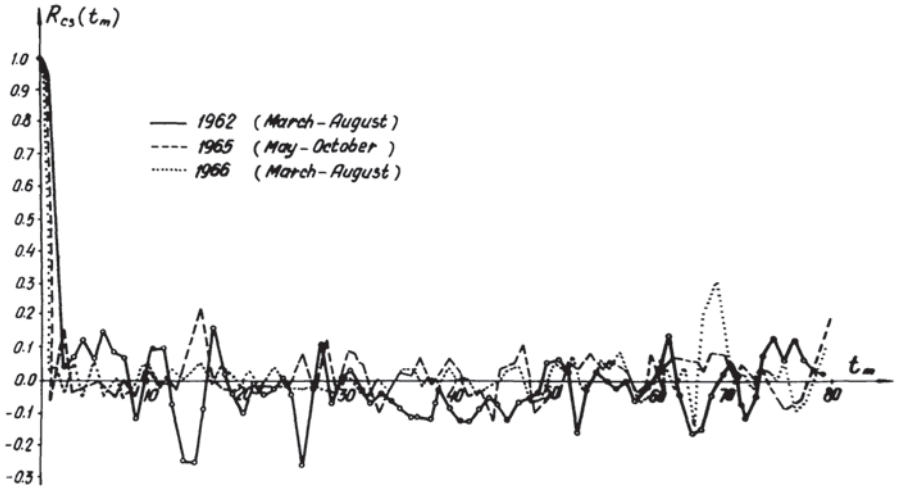

Figure 3.6: Autocorrelation curves of the cross-sections for three periods of five months [22].

from the cross-sections for the three five-month periods for which the most complete experimental evidence was obtained. The principal result, which is illustrated by Figure 3.6, is that no significant periodicity, including a 27 day one, was found. This fact is in complete accordance with the conclusion that the enhanced scattering cross-sections are connected not simply with the existence of the active regions but with definite phases in their evolution [32].

It was also found that the long periods of large scattering cross-sections are connected to simultaneously observed explosive phases of flares. James [41] emphasized particularly the frequent coincidences of the enhanced cross-sections with the rise of the level and the intensification of the fluctuations of sporadic radio emissions of the Sun at 38 MHz. A more extensive analysis of the data connected with the large cross-sections was carried out by Gerasimova (1974) [22]. Usually, large effective cross-sections were observed for several days at times of meridian passage of sunspot groups of a complicated magnetic structure with high flare activity. A high correlation with the total quantity of type III bursts and the continuum connected with type III storms or with noise storms observed in the frequency range (41–8) MHz has been found (Figure 3.7).

Along with cases of the prolonged rise of the scattering cross-sections there were some cases exhibiting isolated rises [42]. These cases coincided with the “birth” of new sunspot groups, or with the rise of flare activity in the already existing active regions. The case of a sudden rise of the cross-section were accompanied by type II bursts, which were followed by the appearance of continuum radio-emissions of type IV and by large quantities of type III bursts.

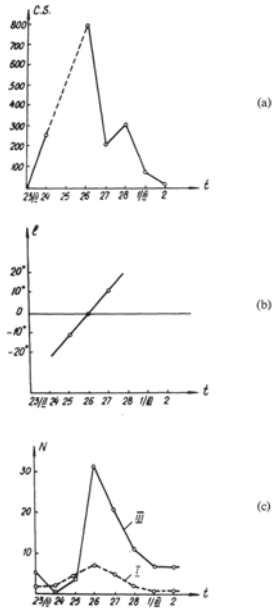

Figure 3.7: Large scattering cross-sections observed during the transit of an active region: (a) Observed cross-sections, (b) Distance from the central meridian, (c) Numbers of the type III and type I radio bursts [22].

When the flare active region appears on the solar disk, the cross-section begins to rise long before its passage through the central meridian. So the indicator of the radio echo cannot always be sharp.

4. Theory of reflections from the Sun

This chapter is devoted to the theory of propagation of radio waves in the solar corona and the mechanisms of reflection (scattering) of these waves.

4.1 Radar equation and scattering cross-section

The fundamental relation between the characteristics of the radar, the target, and the received signal is called the radar equation. The geometry of scattering from an isolated radar target (scatterer) is shown in Figure 4.1, along with the parameters that are involved in the radar equation. Let us consider the simplest case of the vacuum, where the waves will not suffer refraction or absorption. When a power P_t is transmitted by an antenna with gain G_t in the direction of the scatterer, the power density at the scatterer is

$$S_s = \frac{P_t G_t}{4\pi R_t^2}, \tag{4.1}$$

where R_t is the distance from the transmitter to the scatterer. To obtain the total power intercepted by the scatterer, the power density must be multiplied by the effective receiving area of the scatterer:

$$P_{rs} = S_s A_{rs}. \tag{4.2}$$

Note that the effective area A_{rs} is not the actual area of the incident beam intercepted by the scatterer, but rather is the effective area; *i.e.*, it is that area of the incident beam from which all power would be removed if one assumed that the power going through all the rest of the beam continued uninterrupted. The actual value of A_{rs} depends on the effectiveness of the scatterer as a receiving antenna.

Some of the power received by the scatterer is absorbed in losses in the scatterer unless it is a perfect reflector; the rest is reradiated in various directions. If the fraction absorbed is f_a, the fraction reradiated is $1 - f_a$, and the total reradiated power is

$$P_{ts} = P_{rs}(1 - f_a). \tag{4.3}$$

In general, the scattering results in a non-isotropic re-radiation pattern (similar to an antenna pattern) and the gain in the direction of the receiver G_{ts} is the relevant value in the re-radiation pattern. Thus, the energy density at the

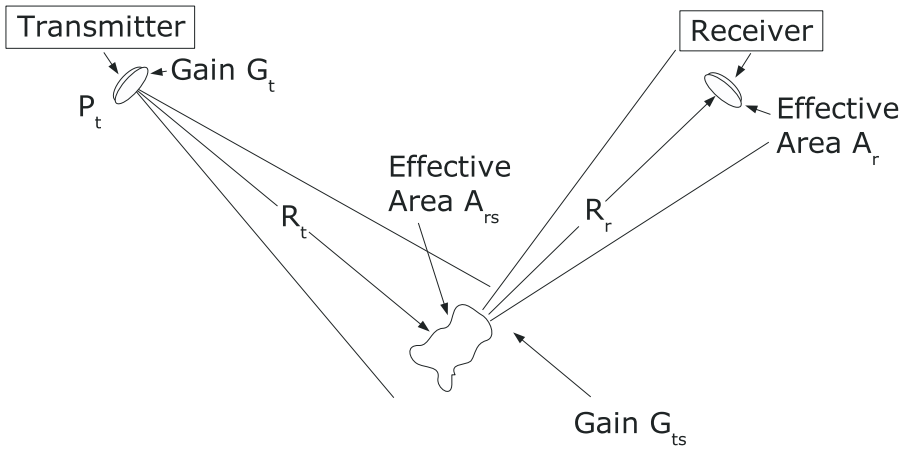

Figure 4.1: The schematic representation of a radar experiment.

receiver is

$$S_r = \frac{P_{ts} G_{ts}}{4\pi R_r^2}, \tag{4.4}$$

where R_r is the distance from the scatterer to the receiver. The power entering the receiver is

$$P_r = S_r A_r = \frac{P_t G_t A_r}{(4\pi)^2 R_t^2 R_r^2} \left[A_{rs} (1 - f_a) G_{ts} \right], \tag{4.5}$$

where A_r is the effective aperture of the receiving antenna, not its actual area. This equation is called the *radar equation*. The factors associated with the scatterer are combined in the square brackets. These factors are difficult to measure individually. Hence, they are normally combined into one factor, the radar *scattering cross-section*:

$$\sigma = A_{rs} (1 - f_a) G_{ts}. \tag{4.6}$$

4.2 Free-free absorption

A radio wave propagating through the solar corona suffers attenuation due to the free-free absorption, and for a radar experiment it is important to estimate the amount of this attenuation. The process of free-free absorption occurs when electrons begin to oscillate in resonance with electric field of a wave and then electron-ion collisions destroy the oscillation. Here we answer the question of how free-free absorption effects energy flux of the emitted radar wave ω_t along its way to the specular reflection point ($\omega_p = \omega_t$) and back, assuming propagation parallel to the plasma density gradient without any refraction.

The absorption of a radio wave along a unit path is given by the coefficient [94]

$$\mu = \frac{1-\varepsilon}{nc}\,\nu_{\text{eff}}, \tag{4.7}$$

where $\varepsilon = 1-\omega_p^2/\omega_t^2$ is the dielectric permittivity, n is the refractive index, c is the speed of light, and ν_{eff} is the effective frequency of collisions of electrons and ions, given by

$$\nu_{\text{eff}} = \frac{5.5N}{T^{3/2}}\,\ln\left[10^4\frac{T^{2/3}}{N^{1/3}}\right], \tag{4.8}$$

where T is the electron temperature, and N is the electron density. The refractive index n is given by

$$n^2 = \varepsilon/2 + \sqrt{(\varepsilon/2)^2 + (2\pi\sigma/\omega_t)^2} \tag{4.9}$$

with

$$\sigma = (1-\varepsilon)\nu_{\text{eff}}/4\pi. \tag{4.10}$$

Evidently, the energy flux for a plane wave is attenuated due to the relation $S = S_0 e^{-\tau(r)}$, where S_0 is the flux outside the corona, τ is the optical depth, and r is the radial distance from the Sun,

$$\tau = \int_{r_0}^{r} \mu(r')dr'. \tag{4.11}$$

Here the integration is done along the wave propagation path. This formula is valid in the approximation of geometrical optics and when the condition

$$|\varepsilon| \gg \nu_{\text{eff}}/\omega_t \tag{4.12}$$

holds.

Figure 4.2 shows the optical depths τ calculated for waves of different frequencies traveling radially towards the Sun. The plasma of the solar corona is assumed to have a density profile described by the Baumbach-Allen model (Equation 2.2) and the electron temperature of $T = 2\times10^6$ K. For easier comparison the abscissa axis does not contain the radial distance from the Sun, r, but the corresponding normalized local plasma frequency $\omega_p(r)/\omega_t$.

The reflection coefficient, taking the absorption for two-way propagation into account, can be written as

$$R^2 = e^{-2\tau_0}, \tag{4.13}$$

where τ_0 is the optical thickness at in the reflection point. For the emitted radio waves with frequencies $\omega_t = 2\pi\times10$, 50 and 100 MHz, the reflection coefficients are $R^2 \approx 0.92$, 0.41 and 0.07, respectively. With this we can conclude that it is preferable to use the lowest possible frequencies for radar probing of the Sun. This, however, will obviously decrease the range of the studied altitudes.

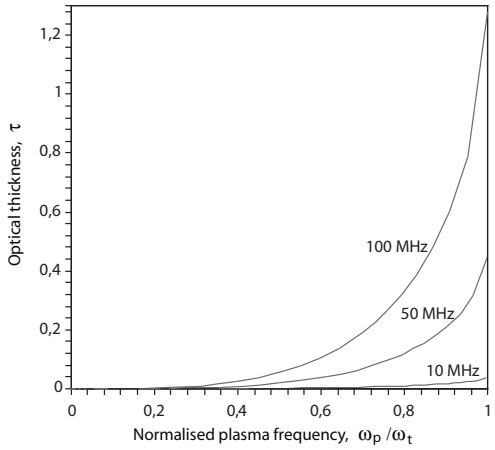

Figure 4.2: Optical depth τ as a function of a normalized plasma density $\omega_p(r)/\omega_t$ for $T = 2 \times 10^6$ K and $\omega_t = 2\pi \times (10; 50; 100)$ MHz.

4.3 Specular reflection

A radio wave propagating towards the Sun will, in general, suffer deviation from its original direction (refraction) together with absorption attenuation. After a time, a wave will encounter an plasma density sufficient to turn it away from the Sun. For a wave propagating along the plasma gradient, this critical density is that which makes the refractive index $n = 0$, whereas for the obliquely propagating wave a smaller electron density will suffice.

Let us assume a spherically symmetric solar corona. Ray trajectories, thus, may be computed using the equation

$$\theta = a \int_{\rho}^{\infty} \frac{d\rho}{\rho \sqrt{n^2 \rho^2 - a^2}}, \tag{4.14}$$

where θ is the angle to a point on the ray measured at the center of the Sun, a is the distance in units of $R_\odot$ between a tangent to the ray at infinity and the center of the Sun, and n is the refractive index at the point (ρ, θ). Ray trajectories for 38 MHz, the Baumbach-Allen model and no-magnetic field case are shown on Figure 4.3. For each ray, the point of closest approach to the photosphere is called the turning point. Note that as a increases, the turning point lies farther out in the corona.

If the reflecting surface were smooth, the reflected signal would be formed from the first Fresnel zone. In reality, the corona is not smooth and the reflecting surface may be considered as rough. Each part of the reflecting surface will contribute something to the backscattered echo, since in each region it will be rays which will meet some $n = 0$ surface normally. To obtain the scattering cross-section of the Sun corresponding to a given frequency, an integration of the energy scattered back into the direction of the observer from

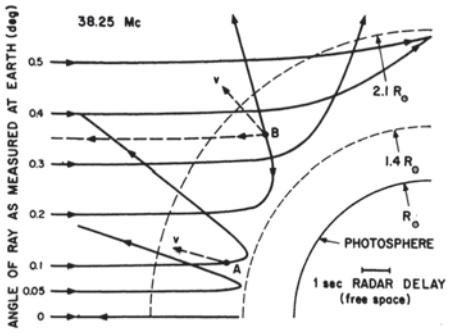

Figure 4.3: Computed ray paths at 38 MHz in a spherically-symmetric corona assuming an Baumbach-Allen density model [41].

all points of the scattering surface must be performed with allowance for the two-way absorption of the signal. Assuming the reflection coefficient being proportional to $\cos^2\theta$ (*Lambert* reflection), or isotropic law give the scattering cross-section of the Sun at 38 MHz of about 1.5 $\pi {R_\odot}^2$.

This theory of specular reflection from a spherically-symmetric solar was introduced by the Australian radio astronomer Kerr [48] and later supplemented by Bass and Braude [4] and James [41].

4.4 Scattering by density fluctuations

This section concerns with the geometrical optics method, which is one of the approximate methods of solving problems involving wave propagation through media containing large-scale random inhomogeneities, whose characteristic dimensions l_ε are large as compared to the wavelength λ [81]. We apply this method in Paper III in order to answer the question of weather density fluctuations in the solar wind and Earth's foreshock strongly diffuse angularly the radar beam on the way to the reflection point and back.

In the process being considered, large-angle scattering (and, in particular, backscattering) is negligible. Fluctuations of the wave field are dominated by those inhomogeneities that lie in the path of the wave, *i.e.*, in the vicinity of the ray connecting the source with the observation point. It is more convenient, therefore, to speak not of scattering but of wave propagation in random media with large-scale random inhomogeneities. Other approximate approaches to fluctuations of shortwave ($\lambda \ll l_\varepsilon$) fields in a random media are the method of smooth perturbations (MSP) and the parabolic equation method (PEM). GOM is the simplest, unlike MPS and PEM, and the most graphic, it does not take into consideration diffraction effects, and is therefore not as versatile as the other two methods. However, within its scope the GOM offers definite advantages. First, in enables a number of effects to be analyzed (*e.g.*, the influence of regular refraction and larger field fluctuations in the vicinity of caustics)

that are not as easily described by the other techniques. Second, some of the results of the method hold even beyond the range of its validity; e.g., phase (but not amplitude) fluctuations and directions of wave propagation.

4.4.1 Geometrical optics equation

The following is a brief derivation of the geometrical optics equation for the simplest case of the scalar monochromatic wave propagation through a medium with stationary continuous inhomogeneities. Suppose that the permittivity $\varepsilon(\mathbf{r})$ in the Helmholtz equation

$$\Delta u + k^2 \varepsilon(\mathbf{r}) u = 0 \tag{4.15}$$

varies only slightly over the wavelength λ ($\lambda|\nabla\varepsilon| \ll \varepsilon$, i.e., the medium is smoothly inhomogeneous). It is natural to assume under these conditions that the field u at each point can be approximated by the plane wave

$$u = Ae^{iS} = Ae^{ik\varphi}, \tag{4.16}$$

where the amplitude A and phase gradient ∇S are slow (in the scale of λ) functions of the coordinates.

Since A and ∇S vary slowly, we can easily derive the equations for A and S or for the quantity $\varphi = S/k$, which is the phase path of the wave and is known as the *eikonal*.

Debye suggested the following derivation of equations for A and φ. We expand A into a series in reciprocals of powers of the wave number

$$u = \left(A_0 + \frac{A_1}{ik} + \frac{A_2}{(ik)^2} + \dots \right) e^{ik\varphi}. \tag{4.17}$$

The coefficients A_m in this expansion are generally complex and, therefore, also contribute to the phase of the resulting field.

Substituting (4.17) into the Helmholtz equation and equating to zero the coefficients at the same powers of k gives the set of equations for φ, A_0, A_1, $A_2 \dots$

$$(k^2) \quad : \quad (\nabla\varphi)^2 = \varepsilon, \tag{4.18}$$

$$(k) \quad : \quad 2(\nabla\varphi\nabla A_0) + A_0\Delta\varphi = 0, \tag{4.19}$$

$$(k^0) \quad : \quad 2(\nabla\varphi\nabla A_1) + A_1\Delta\varphi = -\Delta A_0, \tag{4.20}$$

$$(k^{1-n}) \quad : \quad 2(\nabla\varphi\nabla A_n) + A_n\Delta\varphi = -\Delta A_{n-1}. \tag{4.21}$$

Equation (4.18) is called the *eikonal equation*, and the subsequent equations for $A_n (n = 0, 1, 2, \dots)$ are termed the *transport equations* for the amplitude of the nth approximation. The treatment is generally confined to the zeroth approximation of the GOM, where in (4.17) only A_0 is kept. The higher-order

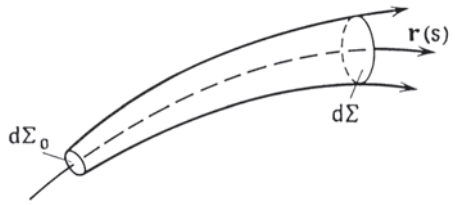

Figure 4.4: A ray tube of infinitesimal thickness [81].

terms in (4.17) are discarded not only because of computational difficulties, but mainly because the series is asymptotic; and it is well known that, with asymptotic expansions, an approximation is not always improved by increasing the number of terms retained.

The eikonal equation (4.18) yields the characteristics (rays) along which the functional $\int \sqrt{\varepsilon} ds$ is extreme (Fermat's principle). Ray equations can be written in different forms. In this treatment it is convenient to represent them in the form

$$\frac{d\mathbf{r}}{ds} = \mathbf{t}, \quad \frac{d\mathbf{t}}{ds} = \frac{1}{2\varepsilon}[\nabla\varepsilon - \mathbf{t}(\mathbf{t}\nabla\varepsilon)], \tag{4.22}$$

where ds is an element of the ray length, and $\mathbf{t}$ is the unit vector tangent to the ray, which doubles as the normal to the phase front $S = k\varphi = const$. Since $|\nabla\varphi| = \sqrt{\varepsilon}$, we have

$$\mathbf{t} = \frac{\nabla S}{|\nabla S|} = \frac{\nabla\varphi}{|\nabla\varphi|} = \frac{\nabla\varphi}{\sqrt{\varepsilon}}.$$

If in some way or other we have found a solution to the ray equations (4.22), the eikonal equation (4.18) and transport equation (4.19) can be integrated along the ray paths. The eikonal φ is found from the Equation

$$\varphi = \int_0^S \sqrt{\varepsilon} ds = \int_0^S \sqrt{\varepsilon[\mathbf{r}(s)]} ds, \tag{4.23}$$

and A_0 from the conservation condition for the intensity $I = \sqrt{\varepsilon} A_0^2$ in the ray tube of infinitesimal thickness and with cross-sectional area $d\Sigma$ (Figure 4.4)

$$Id\Sigma = \sqrt{\varepsilon} A_0^2 d\Sigma = const. \tag{4.24}$$

This relationship follows directly from (4.19), if we write the latter in the form

$$\nabla \cdot (A_0^2 \nabla\varphi) = \nabla \cdot (\sqrt{\varepsilon} A_0^2 \mathbf{t}) = \nabla \cdot (I\mathbf{t}) = 0 \tag{4.25}$$

and integrate over the volume between the cross-sections of the infinitesimally thin ray tube.

We can pass to the geometrical optics approximation (*i.e.*, we can neglect all the terms in (4.17) save for the zeroth) only if the radius of the first Fresnel

zone $\sqrt{\lambda L}$ is small (L is the distance covered by the wave) as compared to the characteristic scale of the inhomogeneities, l_ε,

$$\sqrt{\lambda L} \ll l_\varepsilon. \tag{4.26}$$

We will now turn to random media. It is possible to obtain an analytic solution to the eikonal Equation (4.18) or ray Equation (4.22) for the permittivity ε, which depends on the coordinates in arbitrary way. So here, too, we have to make use of approximate methods, notably of the *perturbation method*. Let $\varepsilon(\mathbf{r}) = \overline{\varepsilon}(\mathbf{r}) + \tilde{\varepsilon}(\mathbf{r})$, where the fluctuational component $\tilde{\varepsilon}$ is small as compared to the regular one ($\sigma_\varepsilon \ll \overline{\varepsilon}$). We represent the eikonal in the form

$$\varphi = \varphi_0 + \varphi_1 + \varphi_2 + \ldots, \tag{4.27}$$

assuming that φ_0 satisfies the "unperturbed" eikonal equation

$$(\nabla\varphi)^2 = \overline{\varepsilon} \tag{4.28}$$

and $|\nabla\varphi_1| \sim \sigma_\varepsilon \ll |\nabla\varphi_0|$, $|\nabla\varphi_2| \sim \sigma_\varepsilon^2 \ll |\nabla\varphi_1|$, and so on. Substituting (4.27) into (4.18) and taking (4.28) into account, for the corrections φ_1, φ_2, ... we get the following linear equations

$$\begin{aligned} 2(\nabla\varphi_0\nabla\varphi_1) &= \tilde{\varepsilon}, \\ 2(\nabla\varphi_0\nabla\varphi_2) &= -(\nabla\varphi_1)^2. \end{aligned} \tag{4.29}$$

Given the unperturbed eikonal φ_0 and unperturbed rays $\mathbf{r}_0 = \mathbf{r}_0(s)$ and $\mathbf{t}_0 = \mathbf{t}_0(s)$ which obey the ray Equations (4.22) at $\varepsilon = \overline{\varepsilon}$, the solutions to these equations can be expressed in quadratures. Note that in a zeroth approximation $\nabla\varphi_0 = \sqrt{\overline{\varepsilon}}\mathbf{t}_0$, where $\mathbf{t}_0 = d\mathbf{r}_0/ds$ is the unit vector tangent to the unperturbed ray $\mathbf{r} = \mathbf{r}_0(s)$. The Equation (4.29) for the first-order correction φ_1, which is generally the only one retained in calculations, will then be

$$2(\nabla\varphi_0\nabla\varphi_1) = 2\sqrt{\overline{\varepsilon}}(\mathbf{t}_0\nabla\varphi_1) = 2\sqrt{\overline{\varepsilon}}\frac{d\varphi_1}{ds} = \tilde{\varepsilon}, \quad \text{hence} \tag{4.30}$$

$$\varphi_1 = \frac{1}{2}\int_0^s \frac{\tilde{\varepsilon}}{\sqrt{\overline{\varepsilon}}} ds'. \tag{4.31}$$

The integration here is along the *unperturbed ray* $\mathbf{r} = \mathbf{r}_0(s)$, i.e., the integrand includes the functions $\tilde{\varepsilon} = \tilde{\varepsilon}[\mathbf{r}_0(s')]$ and $\overline{\varepsilon} = \overline{\varepsilon}[\mathbf{r}_0(s')]$.

4.4.2 Eikonal fluctuations

In a first approximation to the perturbation theory the eikonal is $\varphi \approx \varphi_0 + \varphi_1$. The mean of the first-order correction φ_1 is zero ($\overline{\varphi_1} = 0$), since in the approximation chosen the functional component of the eikonal $\tilde{\varphi} = \varphi - \overline{\varphi}$ coincides with φ_1, and the covariance is

$$\psi_\varphi(\mathbf{r}_1, \mathbf{r}_2) = \langle\tilde{\varphi}(\mathbf{r}_1)\tilde{\varphi}(\mathbf{r}_2)\rangle = \langle\varphi_1(\mathbf{r}_1)\varphi_1(\mathbf{r}_2)\rangle. \tag{4.32}$$

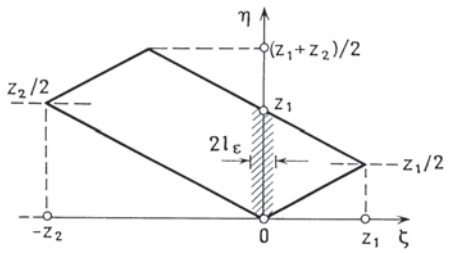

Figure 4.5: Effect of the integration region (shaded) in (4.34) [81].

We will begin with the simplest case. Consider a plane wave $\exp(ikz)$ propagating through a statistically homogeneous medium with mean electric permittivity $\overline{\varepsilon} = 1$. From (4.31), the eikonal covariance is

$$\psi_\varphi(\mathbf{r}_1, \mathbf{r}_2) = \frac{1}{4}\int_0^{z_1} dz' \int_0^{z_2} dz'' \psi_\varepsilon(\boldsymbol{\rho}_1 - \boldsymbol{\rho}_2, z' - z''), \tag{4.33}$$

where $\mathbf{r}_1 = (\boldsymbol{\rho}_1, z_1)$ and $\mathbf{r}_2 = (\boldsymbol{\rho}_2, z_2)$ are the radius vectors of the observation points, and ψ_ε is the covariance of the fluctuations $\tilde{\varepsilon}$. We will now pass in (4.33) to new variables $\zeta = z' - z''$ and $\eta = (z' + z'')/2$. In these variables

$$\psi_\varphi(\mathbf{r}_1, \mathbf{r}_2) = \frac{1}{4}\iint_\Sigma d\zeta d\eta \, \psi_\varepsilon(\boldsymbol{\rho}_1, -\boldsymbol{\rho}_2, \zeta), \tag{4.34}$$

where Σ is the region of integration in the plane (ζ, η). If $z_2 > z_1$, the region is a parallelogram, as shown in (4.5).

The integral (4.34) is dominated by the narrow layer $-l_\varepsilon \lesssim \zeta \lesssim l_\varepsilon$ (shaded in Figure 4.5), where the covariance ψ_ε is markedly distinct from zero. Therefore, the integration limits with respect to ζ can be made infinite, and the integral with respect to η will be taken from 0 to z_1

$$\psi_\varphi(\mathbf{r}_1, \mathbf{r}_2) \approx \frac{1}{4}\int_0^{z_1} d\eta \int_{-\infty}^{\infty} d\zeta \, \psi_\varepsilon(\boldsymbol{\rho}_1 - \boldsymbol{\rho}_2, \zeta) = \frac{z_1}{2}\int_0^{\infty} \psi_\varepsilon(\boldsymbol{\rho}_1 - \boldsymbol{\rho}_2, \zeta) d\zeta.$$

Here we remember that ψ_ε is even in ζ. For $z_2 < z_1$ we would arrive at a similar expression, z_2 being substituted for z_1. Thus

$$\psi_\varphi(\mathbf{r}_1, \mathbf{r}_2) = \frac{z_<}{2}\int_0^{\infty} \psi_\varepsilon(\boldsymbol{\rho}, \zeta) d\zeta, \tag{4.35}$$

where $z_< = \min\{z_1, z_2\}$ is the smaller of z_1 and z_2, and $\boldsymbol{\rho} = \boldsymbol{\rho}_1 - \boldsymbol{\rho}_2$. Specifically, for isotropic fluctuations

$$\psi_\varphi(\mathbf{r}_1, \mathbf{r}_2) = \frac{z_<}{2}\int_0^{\infty} \psi_\varepsilon(\sqrt{\rho^2 + \zeta^2}) d\zeta. \tag{4.36}$$

The eikonal covariance may also be expressed in terms of the spatial spectrum of $\tilde{\varepsilon}$. Substituting into (4.35) the spectral expansion

$$\psi_\varepsilon(\boldsymbol{\rho}, \zeta) = \int_{-\infty}^{\infty} \Phi_\varepsilon(\boldsymbol{\kappa}_\perp, \boldsymbol{\kappa}_z) \exp(i\boldsymbol{\kappa}_\perp \cdot \boldsymbol{\rho} + i\kappa_z \zeta) d^2\kappa_\perp d\kappa_z$$

and integrating with respect to ζ gives

$$\psi_\varphi(\mathbf{r}_1,\mathbf{r}_2)=\frac{\pi z_<}{2}\int_{-\infty}^{\infty}\Phi_\varepsilon(\boldsymbol{\kappa}_\perp,0)\exp(i\boldsymbol{\kappa}_\perp\cdot\boldsymbol{\rho})d^2\kappa_\perp. \tag{4.37}$$

If $\tilde{\varepsilon}$ is isotropic, then $\Phi_\varepsilon(\kappa_\perp,0)=\Phi_\varepsilon\sqrt{\kappa_\perp^2+0^2}=\Phi_\varepsilon(\kappa_\perp)$. If we now change to polar coordinates $\kappa=|\boldsymbol{\kappa}_\perp|=\sqrt{\kappa_x^2+\kappa_y^2},\alpha=\arctan(\kappa_y/\kappa_x)$ and integrate with respect to the angle α, we obtain

$$\psi_\varphi(\mathbf{r}_1,\mathbf{r}_2)=\pi^2 z_<\int_0^\infty\Phi_\varepsilon(\kappa)J_0(\kappa\rho)\kappa d\kappa, \tag{4.38}$$

where $J_0(\kappa\rho)$ is the zeroth-order Bessel function.

4.4.3 Fluctuations of arrival angles

The arrival angles of waves are determined by the direction of the normal to the phase front, which in an isotropic medium coincides with the direction of the unit vector $\mathbf{t}=\nabla\varphi/\sqrt{\varepsilon}$ tangent to the ray. Let us find the deviation of the vector from the unperturbed position $\mathbf{t}_0=\nabla\varphi_0/\sqrt{\varepsilon}$. In a first approximation, we have

$$\mathbf{t}=\frac{\nabla\varphi}{\sqrt{\varepsilon}}=\frac{\nabla(\varphi_0+\varphi_1+\ldots)}{\sqrt{\varepsilon+\tilde{\varepsilon}}}=\frac{\nabla\varphi_0}{\sqrt{\varepsilon}}+\frac{1}{\sqrt{\varepsilon}}\left[\nabla\varphi_1-\frac{\tilde{\varepsilon}\nabla\varphi_0}{2\varepsilon}+\ldots\right].$$

But, by (4.30), $\tilde{\varepsilon}=2\sqrt{\varepsilon}(\mathbf{t}_0\nabla\varphi_1)$, so that

$$\mathbf{t}\approx\mathbf{t}_0+\frac{1}{\sqrt{\varepsilon}}\left[\nabla\varphi_1-\mathbf{t}_0(\mathbf{t}_0\nabla\varphi_1)\right],$$

and the first-order correction to the unperturbed direction $\mathbf{t}_0$ will be

$$\mathbf{t}_1=\mathbf{t}-\mathbf{t}_0=\frac{1}{\sqrt{\varepsilon}}[\nabla\varphi_1-\mathbf{t}_0(\mathbf{t}_0\nabla\varphi_1)]\equiv\frac{\nabla_\perp\varphi_1}{\sqrt{\varepsilon}}, \tag{4.39}$$

where $\nabla_\perp$ is the operator of transverse (relative to the unperturbed ray) differentiation.

From (4.39), $\mathbf{t}_1$ is normal to $\mathbf{t}_0$ and lies in a plane tangent to the unperturbed phase front $\varphi_0=\text{const}$. Let $\boldsymbol{\alpha}$ and $\boldsymbol{\beta}$ be two unit orthogonal vectors in this plane that, together with the vector $\mathbf{t}_0$ tangent to the unperturbed ray, form an orthogonal frame of reference. We can decompose $\mathbf{t}_1$ into two components along the directions $\boldsymbol{\alpha}$ and $\boldsymbol{\beta}$

$$\mathbf{t}_1=t_{1\alpha}\boldsymbol{\alpha}+t_{1\beta}\boldsymbol{\beta}.$$

Up to second-order terms, the arrival angles of the ray θ_α and θ_β, measured from the direction of the unperturbed ray $\mathbf{t}_0$ (Figure 4.6), are $t_{1\alpha}$ and $t_{1\beta}$ respectively

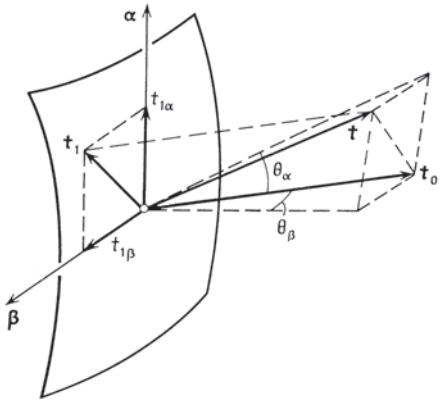

Figure 4.6: Variations of arrival angles in two mutually orthogonal planes [81].

$$\theta_\alpha \approx t_{1\alpha} = \frac{1}{\sqrt{\overline{\varepsilon}}}(\boldsymbol{\alpha}\nabla_\perp\varphi_1) = \frac{1}{\sqrt{\overline{\varepsilon}}}\frac{\partial\varphi_1}{\partial\rho_\alpha}, \quad \theta_\alpha \approx \frac{1}{\sqrt{\overline{\varepsilon}}}\frac{\partial\varphi_1}{\partial\rho_\beta}.$$

It follows that the mean arrival angles in both mutually orthogonal planes $(\mathbf{t}_0, \boldsymbol{\alpha})$ and $(\mathbf{t}_0, \boldsymbol{\beta})$ are zero $(\overline{\theta}_\alpha = \overline{\theta}_\beta = 0)$, as $\overline{\varphi}_1 = 0$ and the elements of the correlation matrix for these angles are given by

$$\psi^\theta_{\alpha\beta}(\boldsymbol{\rho}_1, \boldsymbol{\rho}_2) \equiv \langle \theta_\alpha(\boldsymbol{\rho}_1)\ \theta_\beta(\boldsymbol{\rho}_2)\rangle = \frac{1}{\overline{\varepsilon}}\frac{\partial^2\psi_\perp(\boldsymbol{\rho}_1, \boldsymbol{\rho}_2)}{\partial\rho_{1\alpha}\partial\rho_{1\beta}}. \tag{4.40}$$

We can simplify this equation somewhat by considering that the eikonal fluctuations in a plane tangent to the unperturbed phase front are quasi-homogeneous: the transverse covariance of the eikonal, $\psi_\perp(\boldsymbol{\rho}_1, \boldsymbol{\rho}_2) = \psi_\perp(\boldsymbol{\rho}, \boldsymbol{\rho}_+)$, varies "fast" (on the space scale $\sim l_\varepsilon$) with $\boldsymbol{\rho} = \boldsymbol{\rho}_1 - \boldsymbol{\rho}_2$, and "slowly" (on space scale $L_\varepsilon \gg l_\varepsilon$) with the coordinate of the center of mass $\boldsymbol{\rho}_+ = (\boldsymbol{\rho}_1 + \boldsymbol{\rho}_2)/2$. Therefore, when we pass in (4.40) from $\boldsymbol{\rho}_1$ and $\boldsymbol{\rho}_2$ to $\boldsymbol{\rho}$ and $\boldsymbol{\rho}_+$, we can only differentiate with respect to $\boldsymbol{\rho} = \boldsymbol{\rho}_1 - \boldsymbol{\rho}_2$. If, for simplicity, we discard $\boldsymbol{\rho}_+$ in $\psi^\theta_{\alpha\beta}$ and $\psi_\perp$, we will get

$$\psi^\theta_{\alpha\beta}(\boldsymbol{\rho}) = -\frac{1}{\overline{\varepsilon}}\frac{\partial^2\psi_\perp(\boldsymbol{\rho})}{\partial\rho_\alpha\partial\rho_\beta}. \tag{4.41}$$

Thus, the variances of the arrival angles are given by

$$\langle\theta^2_\alpha\rangle = \psi^\theta_{\alpha\alpha}(0) = -\frac{1}{\overline{\varepsilon}}\frac{\partial^2\psi_\perp(0)}{\partial\rho^2_\alpha}, \quad \langle\theta^2_\beta\rangle = -\frac{1}{\overline{\varepsilon}}\frac{\partial^2\psi_\perp(0)}{\partial\rho^2_\beta}, \tag{4.42}$$

and, in the general case, the anisotropic fluctuations of the eikonal are different.

4.4.4 Coefficient of angular broadening

Here we show how the coefficient of angular broadening $\mu = \langle\theta^2\rangle / z_<$ of a radio wave can be calculated from the power spectrum of density fluctuations. This derivations extend the ones presented in Paper III.

The variance of the arrival angle for isotropic fluctuations can be obtained by substituting the eikonal correlation function from (4.38) into (4.42) at $\rho \to 0$

$$\langle\theta^2\rangle = -\frac{\pi^2 z_<}{\overline{\varepsilon}} \int_0^\infty \Phi_\varepsilon(\kappa)\kappa \frac{\partial^2 J_0(\kappa\rho)}{\partial\rho^2} d\kappa \Bigg|_{\rho\to 0}, \tag{4.43}$$

where $\Phi_\varepsilon(\kappa)$ is a 3D spectrum of permittivity. The second derivative of the Bessel function is

$$\frac{\partial^2 J_0(\kappa\rho)}{\partial\rho^2} = \kappa^2 \left(\frac{J_1(\kappa\rho)}{\kappa\rho} - J_0(\kappa\rho) \right). \tag{4.44}$$

The argument $\kappa\rho$ in the limit $\rho \to 0$ in the general case does not approach zero (because κ changes in $0 \leqslant \kappa \leqslant \infty$), but assuming that the spectra of permittivity vanishes at small scales ($\Phi_\varepsilon(\kappa) = 0$ for $\kappa > \kappa_{\max}$) it always does. Using the expansion

$$J_n(\delta) = \frac{\delta^n}{2^n n!} \left\{ 1 - \frac{\delta^2}{2(2n+2)} + \ldots \right\}$$

we get

$$\frac{\partial^2 J_0(\kappa\rho)}{\partial\rho^2} \Bigg|_{\kappa\rho\to 0} = \kappa^2 \left(\frac{1}{2} - 1 \right) = -\frac{\kappa^2}{2}. \tag{4.45}$$

Thus the variance becomes

$$\langle\theta^2\rangle = \frac{\pi^2 z_<}{2\overline{\varepsilon}} \int_0^{\kappa_{\max}} \Phi_\varepsilon(\kappa)\kappa^3 d\kappa. \tag{4.46}$$

The 3D power spectrum of electric permittivity is related to the 1D power spectrum of density fluctuations by

$$\Phi_\varepsilon(\mathbf{k}) = \frac{1}{4\pi} \frac{\Phi_N(k)}{N_0^2} k^{-2}, \tag{4.47}$$

where N_0 is a density of plasma with plasma frequency equal to the frequency of a radio wave ω_t,

$$N_0 = \frac{\omega_t^2 m_e}{4\pi e^2}. \tag{4.48}$$

Assuming the spectrum of density fluctuations of the power law form

$$\Phi_N(k) = \overline{N}^2 \times a \times (k\rho_i)^{-b}, \tag{4.49}$$

where ρ_i is the ion thermal gyroradius, yields the coefficient of angular broadening

$$\mu = \frac{\pi}{8\overline{\varepsilon}\rho_i^2}\left(\frac{\overline{N}}{N_0}\right)^2 \frac{a\,(k\rho_i)^{2-b}}{2-b}\Bigg|_{k_{min}\rho_i}^{k_{max}\rho_i} = \frac{\pi}{8\overline{\varepsilon}\rho_i^2}\frac{\omega_p^4}{\omega_t^4}\frac{a\,(k\rho_i)^{2-b}}{2-b}\Bigg|_{k_{min}\rho_i}^{k_{max}\rho_i}. \qquad (4.50)$$

4.4.5 Application to the El Campo experiments

Scattering by density fluctuations as the possible mechanism explaining the El Campo experiment was considered by Chashei and Shishov [11]. These authors assume scattering of a $\lambda = 8$ m (38 MHz) radio wave by MHD waves propagating from the base of corona [12] having the 3D power spectrum of density fluctuations

$$\Phi_N(\mathbf{k}) = C_N k^{-3}, \qquad (4.51)$$

with the cutoff at the smallest scale $l = 2\pi/k_{\max} \approx 10^5$ cm. The coefficient of angular broadening is assumed to depend on the altitude in the corona as

$$\mu = \mu_0 (r_0/r)^{\nu}, \qquad (4.52)$$

where μ_0 and r_0 are scaling factors. From the condition

$$\mu_0 \int_{r_0}^{r} \left(\frac{r_0}{r}\right)^{\nu} dr \approx 1, \qquad (4.53)$$

and the temporal parameters of a reflected pulse from the El Campo experiments it is estimated that reflections may occur at altitudes of $\approx 2\ R_\odot$ with scattering cross-section of $\approx 10\ \pi {R_\odot}^2$. The authors also conclude that the scattering by density fluctuations is more effective than the surface specular reflection only for radar signals of sufficiently long wavelength ($\lambda > 4$ m).

4.5 Induced scattering by wave turbulence

As the El Campo experimental results could not be explained within the framework of specular reflection theory, and it was proposed that the radar echo can be formed due to the process of induced scattering by a wave turbulence.

We may explain the physical picture of this process by the example of induced scattering of a electromagnetic wave by the plasma (Langmuir) turbulence. An electromagnetic wave t in the presence of an longitudinal plasma wave l may emit a longitudinal wave with transition to an electromagnetic wave of different wave vector and frequency t' ($t \to l + t'$), see Figure 4.7. The inverse process of absorption of a longitudinal plasma wave l by the electromagnetic wave t' with a transition to t ($l + t' \to t$) may also occur. These processes are called *decay* and *coalescence* respectively. They are described,

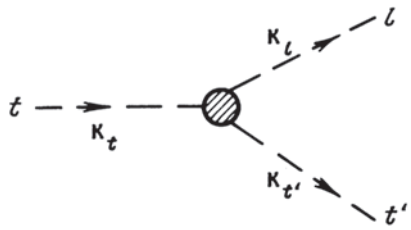

Figure 4.7: Decay of a transverse wave t into a longitudinal l and a transverse wave t'.

in the random phase approximation, by the following kinetic wave equations [89]:

$$\frac{dN^t_{\mathbf{k_t}}}{dt} = -\int \tilde{w}(\mathbf{k_l},\mathbf{k_t},\mathbf{k_{t\prime}})\frac{d\mathbf{k_l}d\mathbf{k_{t\prime}}}{(2\pi)^6}(N^t_{\mathbf{k_t}}N^t_{\mathbf{k_{t\prime}}} - N^t_{\mathbf{k_{t\prime}}}N^l_{\mathbf{k_l}} + N^t_{\mathbf{k_t}}N^l_{\mathbf{k_l}}), \quad (4.54)$$

$$\frac{dN^t_{\mathbf{k_{t\prime}}}}{dt} = \int \tilde{w}(\mathbf{k_l},\mathbf{k_t},\mathbf{k_{t\prime}})\frac{d\mathbf{k_l}d\mathbf{k_t}}{(2\pi)^6}(N^t_{\mathbf{k_t}}N^t_{\mathbf{k_{t\prime}}} - N^t_{\mathbf{k_{t\prime}}}N^l_{\mathbf{k_l}}N^t_{\mathbf{k_t}}N^l_{\mathbf{k_l}}),$$

where $N^t_{\mathbf{k_t}}$, $N^t_{\mathbf{k_{t\prime}}}$, and $N^l_{\mathbf{k_l}}$ are the number densities of electromagnetic and longitudinal wave quanta, $\tilde{w}(\mathbf{k_l},\mathbf{k_t},\mathbf{k_{t\prime}})$ is the probability of emission of $\mathbf{k_l}$ by $\mathbf{k_t}$ with transition into $\mathbf{k_{t\prime}}$ which is equal to the probability of absorption of $\mathbf{k_l}$ by $\mathbf{k_{t\prime}}$ with transition into $\mathbf{k_t}$. Number density of quanta $N_\mathbf{k}$ is related to a spectral energy density of the turbulence $W_\mathbf{k}$ as

$$N_\mathbf{k} = \frac{W_\mathbf{k}}{\hbar\omega}, \quad (4.55)$$

where $\mathbf{k}$ and ω are wave vector and frequency, respectively; and the energy density of the turbulence W is related to the spectral energy density as

$$W = \int W_\mathbf{k}\frac{d^3k}{(2\pi)^3}. \quad (4.56)$$

The kinetic wave equations (4.54) are valid only in the weak turbulence limit, which basically requires the energy density of the turbulence to be much less than the thermal energy density of the plasma [14],

$$\frac{W}{nT} < (k_l\lambda_D)^2, \quad (4.57)$$

where n and T are the electron plasma density and temperature, and λ_D is the electron Debye length.

The coalescence and decay processes must comply with the laws of the momentum and energy conservation (so called "resonant conditions")

$$\hbar\mathbf{k_t} = \hbar\mathbf{k_l} + \hbar\mathbf{k_{t\prime}}, \quad (4.58)$$

$$\hbar\omega_t = \hbar\omega_l + \hbar\omega_{t\prime}, \tag{4.59}$$

which are present as Dirac delta functions in a probability coefficient. We may notice that after a decay, the electromagnetic wave frequency decreases with an amount which equals the frequency of the scattering wave and after coalescence it increases by the same amount.

The radar wave when propagating through a region "filled" with the plasma turbulence, assuming the resonant conditions to be satisfied, generates satellite waves at frequencies $\omega_t \pm \omega_l$. The equation which describes the loss of intensity of the radar wave due to satellite line generation, taking also into account the inverse process of re-scattering of satellites back to ω_t, may be written as follows:

$$\begin{aligned}\frac{dN^t_{\mathbf{k_t}}}{dt} &= \int \tilde{w}(\mathbf{k_l},\mathbf{k_{t\prime\prime}},\mathbf{k_t})\frac{d\mathbf{k_l}d\mathbf{k_{t\prime\prime}}}{(2\pi)^6}(N^t_{\mathbf{k_t}}N^t_{\mathbf{k_{t\prime\prime}}}+N^t_{\mathbf{k_{t\prime\prime}}}N^l_{\mathbf{k_l}}-N^t_{\mathbf{k_t}}N^l_{\mathbf{k_l}})- \\ &- \int \tilde{w}(\mathbf{k_l},\mathbf{k_t},\mathbf{k_{t\prime}})\frac{d\mathbf{k_l}d\mathbf{k_{t\prime}}}{(2\pi)^6}(N^t_{\mathbf{k_t}}N^t_{\mathbf{k_{t\prime}}}-N^t_{\mathbf{k_{t\prime}}}N^l_{\mathbf{k_l}}+N^t_{\mathbf{k_t}}N^l_{\mathbf{k_l}}).\end{aligned} \tag{4.60}$$

Here the first integral accounts for the $t+l \rightleftarrows t''$ and the second accounts for the $t \rightleftarrows l+t'$ process.

Let the intensity of the satellites $\mathbf{k_{t\prime}}$ and $\mathbf{k_{t\prime\prime}}$ be much smaller than the intensity of the incident wave $\mathbf{k_t}$. Then, in Equation 4.60 we can drop terms containing $N^t_{\mathbf{k_{t\prime}}}$ and $N^t_{\mathbf{k_{t\prime\prime}}}$

$$\frac{dN^t_{\mathbf{k_t}}}{dt} = -\int\left[\tilde{w}(\mathbf{k_l},\mathbf{k},\mathbf{k_t})N^l_{\mathbf{k_l}}N^t_{\mathbf{k}}+\tilde{w}(\mathbf{k_l},\mathbf{k_t},\mathbf{k})N^l_{\mathbf{k_l}}N^t_{\mathbf{k}})\right]\frac{d\mathbf{k_l}d\mathbf{k}}{(2\pi)^6}. \tag{4.61}$$

The first term describes the appearance of the "red" satellite and the second describes the "blue" satellite. The probability of the process of decay and coalescence is proportional to the intensity of the waves which are already existing. It is a characteristic feature of induced processes of scattering that they lead to an exponential rise of the satellites intensity.

The same mechanism as we have considered, works not only for plasma waves, but also for other wave modes, e.g., upper-hybrid, Bernstein, Z mode, lower-hybrid, Alfvén, whistler, or ion-sound waves. The radar wave and the echo may also be considered as being an O mode and/or an X mode wave.

In principle, more complicated processes are possible, in which the radar wave transforms into three other waves, or the radar wave and another wave transform into two other waves.

The mechanism of formation of the echo due to induced scattering by wave turbulence was considered in a number of articles. This includes scattering by *isotropic* ion-sound turbulence [30, 31, 33, 34], isotropic Langmuir turbulence [35], and lower-hybrid waves [92]. Scattering by the *anisotropic* Langmuir and ion-sound turbulence, is studied in [59, 58, 60], Paper I, and Paper II.

5. Summary of the papers

This chapter contains a brief summary of the publications included in this thesis.

Paper I. Combination scattering by anisotropic Langmuir turbulence with application to solar radar experiments.

In this paper we study the feasibility of radar detection of an anisotropic Langmuir turbulence in the solar corona due to a nonlinear scattering process $t + l \rightleftarrows t$. The turbulence is assumed to be generated by electrons, responsible for type III solar radio burst, which propagate towards the radar site. These electrons generate Langmuir waves with wave vectors quasi-parallel and antiparallel to the propagation direction. Using wave-kinetic theory we obtain expressions for the frequency shift, the scattering cross-section, the coefficient of absorption (due to scattering), and the optical depth, which result in an estimate for the echo spectrum. We show that i) the optical depth can exceed unity, which means that the process considered is efficient, ii) the turbulence can have large scattering cross-section $\sigma \gg \pi {R_\odot}^2$, iii) the frequency shift of the scattered signal lies in the range $-\omega_t/2 < \Delta\omega \lesssim -\omega_t/8$ and $\omega_t/7 \lesssim \Delta\omega \leqslant \omega_t$, where ω_t is the frequency of the radar signal, and iv) the efficiency of the scattering process (the coefficient of absorption) increases with the increase of ω_t.

Paper II. Radar detection of interplanetary shocks: scattering by anisotropic Langmuir turbulence.

Earth-directed interplanetary shocks associated with Coronal Mass Ejections (CMEs) are known to have a severe impact on the magnetosphere, causing geomagnetic storms and substorms. Thus, early detection of such shocks is very important. The feasibility of radar detection of an interplanetary shocks is studied. The reflection mechanism considered is based on the induced scattering $t + l \rightleftarrows t$ of a radar wave by an anisotropic Langmuir turbulence, which is generated by shock accelerated electrons. We focus on the dependence of the scattering process on the angle between the electron beam and the radar wave, $\mathbf{v}_b \hat{} \mathbf{k_t}$ (extending the theory presented in Paper I, where only the particular case of $\mathbf{v}_b \hat{} \mathbf{k_t} = \pi$ is considered). Using wave-kinetic theory we obtain expressions for the frequency shift, the scattering cross-section, the coefficient of absorption (due to scattering), and

the optical depth. These parameters show strong dependence on the angle $\mathbf{v}_b\hat{}\mathbf{k_t}$ for the process of decay ($t \rightarrow t' + l$), and relatively weak dependence for the process of coalescence ($t + l \rightarrow t'$). The altitudes in the solar corona, where scattering is allowed are different for the decay and coalescence processes. If expressed in the local plasma frequency, the altitudes span the range $\omega_t/7 \lesssim \omega_p \leqslant \omega_t$ for $\mathbf{v}_b\hat{}\mathbf{k_t} = \pi$ and $\omega_t/120 \lesssim \omega_p \leqslant \omega_t$ for $\mathbf{v}_b\hat{}\mathbf{k_t} = \pi/2$, for the coalescence process (ω_t is the frequency of the radar signal). For the decay $\omega_t/8 < \omega_p \lesssim \omega_t/2$ for $\mathbf{v}_b\hat{}\mathbf{k_t} = \pi$ and for $\mathbf{v}_b\hat{}\mathbf{k_t} = \pi/2$ the decay does not occur at all. It is essential that the region of scattering moves significantly closer to the radar with a decrease in the $\mathbf{v}_b\hat{}\mathbf{k_t}$ angle. In this case the radar signal is scattered at an angle to the radar, thus, its detection must be done in a remote location. If transmitting from the Earth the scattered signal can be detected, for example, by a satellite or on the moon. A successful experiment at the radar frequency $\omega_t = 2\pi \times 100$ MHz, requires the energy density of the turbulence to exceed $W = 10^{-5}\ nT$ (nT is the thermal energy density of a plasma), which is quite realistic according to our estimations.

Paper III. Scattering of radio waves by density fluctuations in the solar wind and terrestrial foreshock.

The radio beam emitted by a solar radar propagates through a number of different media on its way to the reflection point and back: the ionosphere, the magnetosphere, the Earth's foreshock, and the solar wind. In this paper we estimate the angular broadening of a radar beam caused by density fluctuations in the terrestrial ion and electron foreshocks and the unperturbed solar wind. The power spectra of density fluctuations in these regions are obtained from Cluster satellite data. These spectra are used to calculate coefficients of angular broadening of a radio wave in the regions studied. Minimum broadening is expected in the unperturbed solar wind and maximum in the ion foreshock. The results suggest that total angular broadening will not seriously affect the probing of the Sun by the radar beam. The density fluctuations play an important role also in other physical phenomena (plasma wave generation, propagation and interaction), thus, the density fluctuations spectra obtained can have a broader use.

Paper IV. In situ observation of type II solar radio burst source region: a new generation mechanism.

Type II solar radio bursts are known to be associated with interplanetary shocks travelling through the space plasma. It is widely accepted that the radio emission itself occurs as a final step in a series of physical processes: particle acceleration on the shock, generation of plasma waves, and finally conversion of plasma waves into electromagnetic

waves (plasma emission mechanism). The conclusions about such mechanism are drawn mainly on the basis of remote observation of the radiation, and there is clearly a lack of in situ observations of the source region. In this paper we present in situ satellite observation of a type II solar radio burst associated with a CME-driven interplanetary shock. The intense emissions above the electron plasma frequency are observed along with energetic electron beams in close vicinity of the ramp of the shock. On the basis of the observations and analytical calculations we suggest that the generation is taking place locally at the shock front and just behind it and we propose a possible generation mechanism. The mechanism is related to the energetic particles passing the shock front, known in electrodynamics as transition radiation.

6. Summary in Ukrainian

Стислий виклад українською

Ця дисертація присвячена теорії радіолокації Сонця. На Сонці відбувається широкий спектр фізичних явищ, причому деякі з них, такі як нагрів сонячної корони та прискорення сонячного вітру, є досі незрозумілими або не до кінця зрозумілими. Дослідження Сонця ведеться головним чином виходячи із спостережень його випромінювання. Ідеї щодо використання радару для вивчення Сонця з'явилися у 40-х роках минулого сторіччя одночасно з першими успішними експериментами з радіолокації Місяця [68, 5]. Теоретичною основою для експериментів з радіолокації Сонця стали роботи В. Гінзбурга (1946) [23], Ф. Керра (1952) [48], та Ф. Басса і С. Брауде (1957) [4], в яких отримані оцінки параметрів відбитого сигналу та необхідні характеристики радара. Перший експеримент з радіолокації Сонця було проведено в 1959 році групою зі Стенфордського Університету [18]. Перші систематичні експерименти проводилися з 1961 по 1969 рік, групою з Масачусецького Технологічного Інституту, на чолі з Джесі Джеймсом, за допомогою спеціально побудованої радарної установки біля м. Ель Кампо, штату Техас [42]. Решта експериментів з радіолокації Сонця були безуспішними. Таким чином, експерименти Дж. Джеймса залишаються до цього часу єдиним джерелом експериментальних даних.

Результати отримані Дж. Джеймсом виявилися в більшій своїй мірі неочікуваними. Спочатку вважалося, що радіолокаційний сигнал буде відбиватися від шару з нульовим індексом заломлення (так зване, дзеркальне відбиття), що відповідає висоті в сонячній короні 1.6 $R_\odot$, та мати інтенсивність, що виражається через переріз розсіяння, порядку 1.5 $\pi {R_\odot}^2$, де $R_\odot$ є радіусом Сонця. Проте, відбиття, що спостерігалися, приходили з різних висот, від -2.6 $R_\odot$ (відбиття зі зворотньої сторони Сонця) до 5 $R_\odot$. Перерізи розсіяння змінювалися щодня, від менш ніж $\pi {R_\odot}^2$ до декількох сотень $\pi {R_\odot}^2$. Стало зрозумілим, що модель дзеркального відбиття не може пояснити спостереження, та, що відбиття (розсіяння) повинно відбуватися за рахунок більш складних процесів взаємодії радіолокаційного сигналу з турбулентністю в сонячній короні.

Процес розсіяння радіосигналу хвильовою турбулентністю інтенсивно вивчається в лабораторних та іоносферних радарних експериментах. Останні дуже подібні до сонячних радарних експериментів, і можуть бути вельми корисними. В іоносфері, як і в сонячній короні наявні магнітне поле та градієнти густини плазми. Турбулентність в іоносфері може генеруватися як природним чином, – струмом вздовж магнітного поля, так і штучним, – шляхом опромінення плазми потужною високочастотною радіохвилею (нагрівний експеримент). В сонячній короні турбулентність генерується потоками високоенергетичних електронів, що прискорюються на Сонці, або на фронті ударної хвилі. Про наявність потоків таких електронів та турбулентності у сонячній короні свідчить пов'язане з ними радіовипромінювання, яке називається сонячними радіосплесками.

Програма космічної погоди[1] останнім часом стимулювала зацікавленість у експериментах з радіолокації Сонця, переслідуючи мету завчасного виявлення викидів корональних мас (ВКМ), що рухаються у напрямку Землі. Такі геоефективні ВКМ можуть бути небезпечними для життя космонавтів, пошкоджувати супутники, викликати потужні геомагнітні бурі, які, в свою чергу, призводять до порушення радіозв'язку, руйнуваня ліній електропередач та від'єднаня від електропостачання величезних територій [80]. Опис експериментальних пропозицій з радіолокації Сонця можна знайти у посиланнях [87, 13, 78]. Імовірно, що нові радарні експерименти з використанням сучасних технологій передачі, прийому та обробки сигналу, в поєднанні з сучасними можливостями спостережень в оптичному, ультрафіолетовому, та рентгенівському діапазонах, зроблять вагомий внесок в наше розуміння фізики Сонця.

Ця дисертація складається з двох частин. Перша частина містить огляд експериментів та теорії радіолокації Сонця. Друга – чотири статті, які є особистим внеском автора та його колег до цієї теорії.

Стаття I. Комбінаційне розсіяння анізотропною ленгмюрівською турбулентністю із застосуванням до експериментів з радіолокації Сонця.

В цій статті вивчається можливість детектування радаром анізотропної ленгмюрівської турбулентності в короні Сонця за рахунок процесу нелінійного розсіяння $t + l \rightleftarrows t$. Вважається, що турбулентність генерується потоком електронів, що відповідає за радіосплеск III типу, причому електрони рухаються в напрямку на радар. Такий потік генерує первинні ленгмюрівські хвилі з хвильовими векторами переважно

[1] Див., наприклад, http://www.spaceweather.com

вздовж напрямку руху електронів. Частина первинних хвиль змінює напрямок розповсюдження на протилежний в процесі розсіяння тепловими іонами ($l + i \rightleftarrows l + i$), або іонно-звуковими хвилями ($l + s \rightleftarrows l$). Використовуючи кінетичну теорію нелінійної взаємодії хвиль отримуються вирази для частотних зсувів розсіяного радіолокаційного сигналу, перерізу розсіяння, коефіцієнта поглинання радарної хвилі (за рахунок розсіяння) та оптичної товщі. На їх основі розраховуються спектри розсіяного сигналу. Отримані результати обговорюються в рамках застосування до радарного експерименту. Показано, що і) оптична товща може перевищувати одиницю, тобто процес $t + l \rightleftarrows t$ є ефективним, іі) турбулентність може мати великі перерізи розсіяння ($\sigma \gg \pi {R_\odot}^2$), ііі) частотний зсув розсіяного сигналу лежить у межах $-\omega_t/2 < \Delta\omega \lesssim -\omega_t/8$ та $\omega_t/7 \lesssim \Delta\omega \leqslant \omega_t$, де ω_t - частота радіолокаційного сигналу, та іv) ефективність розсіяння (коефіцієнт поглинання) збільшується при збільшені частоти ω_t.

Стаття II. Радіолокація міжпланетних ударних хвиль: розсіяння анізотропною ленгмюрівською турбулентністю.

Програма сонячної погоди приділяє особливу увагу завчасному виявленню викидів корональної маси (ВКМ), що розповсюджуються в напрямку до Землі. Деякі ВКМ створюють ударну хвилю, що прискорює електрони, які, в свою чергу, генерують ленгмюрівську турбулентність в областях попереду та позаду фронту ударної хвилі. В цій статті досліджується можливість виявлення міжпланетних ударних хвиль з допомогою радарних експериментів за рахунок розсіяння радіолокаційного сигналу ленгмюрівською турбулентністю (процес $t + l \rightleftarrows t$). Особлива увага приділяється вивченню залежності процесу розсіянні від кута між напрямком розповсюдження електронів та радіолокаційного сигналу, $\mathbf{v}_b \hat{} \mathbf{k_t}$, (на відміну від Статті I, де розглядається частинний випадок, $\mathbf{v}_b \hat{} \mathbf{k_t} = \pi$). Використовуючи кінетичну теорію нелінійної взаємодії хвиль знайдено вирази для частотних зсувів розсіяного радіолокаційного сигналу, перерізу розсіяння, коефіцієнта поглинання радарної хвилі (за рахунок розсіяння) та оптичної товщі. Ці параметри суттєво залежать від кута $\mathbf{v}_b \hat{} \mathbf{k_t}$ для процесу розпаду ($t \rightarrow t' + l$), та майже не залежать для процесу злиття ($t + l \rightarrow t'$). Так, межі частотного зсуву розсіяного сигналу для процесу розпаду змінюються від $-\omega_t/2 < \Delta\omega \lesssim -\omega_t/8$ при $\mathbf{v}_b \hat{} \mathbf{k_t} = \pi$ до $0 < \Delta\omega < 0$ при $\mathbf{v}_b \hat{} \mathbf{k_t} = \pi/2$. Для процесу злиття границі змінюються

від $\omega_t/7 \lesssim \Delta\omega \leqslant \omega_t$ при $\mathbf{v}_b\hat{}\mathbf{k_t} = \pi$ до $\omega_t/120 \lesssim \Delta\omega \leqslant \omega_t$ при $\mathbf{v}_b\hat{}\mathbf{k_t} = \pi/2$. Важливо відзначити, що величина частотного зсуву дорівнює локальній плазмовій частоті шару де відбулося розсіяння, тому при зменшенні кута $\mathbf{v}_b\hat{}\mathbf{k_t}$ область, де може відбуватися розсіяння значно наближається до радару. При цьому, розсіяння відбувається під кутом до передавача, а отже, прийом повинен здійснюватися на значних відстанях від передавача. У випадку локації з Землі, розсіяний сигнал можна реєструвати, наприклад, на супутнику. Для успішної локації на частоті $\omega_t = 2\pi \times 100$ МГц, густина енергії турбулентності має перевищувати $W = 10^{-5}\ nT$ (nT - теплова густина енергії плазми), що за оцінками є досить реалістичним.

Стаття III. Розсіяння радіохвиль флуктуаціями густини в сонячному вітрі та в області магнітно з'єднаної з фронтом ударної хвилі Землі (форшоку).

Відомо, що розсіяння радіо хвиль при проходженні через плазму з флуктуаціями густини впливає на видимий кутовий розмір радіоджерела та викликає сцинціляції інтенсивності та збільшення кутової дисперсії. Радіолокаційний сигнал, на своєму шляху до місця відбиття (розсіяння), а також на зворотньому шляху, проходить через декілька областей, з різними фізичними характеристиками. Це іоносфера, магнітосфера, форшок Землі та сонячний вітер. В цій статті оцінюється збільшення кутової дисперсії радіолокаційного сигналу, що спричинено флуктуаціями густини плазми у незбуреному сонячному вітрі та електронному та іонному форшоках. Спектри флуктуацій густини у цих областях розраховуються на основі експериментальних даних з супутників проекту Кластер (Cluster). Ці спектри використовуються для розрахунку коефіцієнтів кутового розширення радіохвилі в областях, які вивчаються. Мінімальна кутове розширення очікується у незбуреному сонячному вітрі та максимальне – в іонному форшоці. З результатів випливає, що повний ефект кутового розширення не суттєвий для експериментів з радіолокації Сонця. Флуктуації густини плазми впливають на процесіи герерації хвиль, їх розповсюдження та взаємодію, тому отримані спектри флуктуацій можуть мати більш широке застосування.

Стаття IV. Локальні спостереження сонячного рідіосплеску II типу: новий механізм генерації.

Сонячні радіосплески II типу асоціюються з ударними хвилями, що розповсюджуються від Сонця. Загальноприйнято, що радіовипромінення відбувається на кінцевому етапі ланцюжку фізичних процесів: прискорення електронів ударною хвилею, генерація ленгмюрівських хвиль та, зрештою, конвертація ленгмюрівських хвиль у радіохвилі (плазмовий механізм випромінення). Висновок стосовно цього механізму був зроблений переважно на підставі віддалених спостережень випромінення. Існує очевидна нестача локальних спостережень області джерела. Ця стаття представляє супутникові локальні спостереження сонячного радіосплеску II типу, пов'язаного з ударною хвилею, яка розповсюджується перед ВКМ. Інтенсивне випромінення з частотою більшою за плазмову частоту спостерігається одночасно з потоками субрелятивістських електронів безпосередньо біля фронту ударної хвилі. На підставі спостережень та аналітичних розрахунків, автори стверджують, що генерація відбувається локально на фронті ударної хвилі та пропонують новий механізм генерації. Цей механізм, пов'язаний з перетином енергетичнми частинками фронту ударної хвилі, відомий в електродинаміці як перехідне випромінювання.

7. Summary in Swedish

Sammanfattning påsvenska

En allmän metod som används för att undersöka okända objekt i ett fysiklaboratorium är att bestämma objektets spridningsegenskaper efter det att man bestrålat det med partiklar eller vågor. Denna metod används inom radarastronomi (radiodetektion och avståndsbestämning) för att studera himlakroppar, inom meteorologi, jonosfärsfysik och många andra områden inom fysiken. En radar sänder elektromagnetiska vågor i den riktning som definieras av antennsystemet och registrerar en reflekterad (spridd) signal från objekt som ligger i radarstrålens väg. Energiflödet i den utsända strålen avtar som kvadraten av avståndet från sändaren, och det reflekterade energiflödet avtar på samma sätt. På grund av detta kommer förmodligen metoden att studera objekt med hjälp av radar att för alltid vara begränsad till vårt solsystem.

En mängd olika fysiska fenomen upptrder i och på solen, varav vissa fortfarande knappt eller inte alls är förklarade, till exempel uppvärmningen av koronan eller accelerationen av solvinden. Man studerar huvudsakligen solen genom att undersöka dess strålning. Idén att studera solen med hjälp av radar uppkom runt 1940 i samband med det första lyckade experimentet att detektera en himlakropp, månen [68, 5]. Den teoretiska grunden för radarexperiment av solen lades av Ginzburg (1946) [23], Kerr (1952) [48], och Bass och Braude (1957) [4], som gjorde en uppskattning det förväntade ekot och de nödvändiga radarparametrarna. Det hävdas att de första reflektionerna från solen observerades 1959 av en grupp vid Stanford universitetet som använde en radar som opererade vid 25 MHz [18]. De första systematiska radarexperimenten utfördes från 1961 till 1969 av en MIT grupp ledd av Jesse James vid den välkända solradar faciliteten El Campo, Texas [42]. Alla övriga solradarexperiment har hittills misslyckats. Därför förblir experimenten utförda med El Campo radarn den enda källan till solekodata till dags dato.

Resultaten som erhölls vid El Campo var till stor del oväntade. Från början antog man att ekona skulle komma från ett skikt vars refraktionsindex var noll (så kallad spekulär reflektion). Det skulle motsvara en höjd omkring 1.6 $R_\odot$ i solens korona och borde ha en intensitet, uttryckt i spridningstvärsnittet, på ungefär 1.5 $\pi {R_\odot}^2$, där $R_\odot$ är solens radie. Emellertid visade det sig att de observerade ekona kom från olika höjder, allt från $-2.6\ R_\odot$ (reflektion från baksidan av solen) till 5 $R_\odot$. De observerade värdena på tvärsnitten varierade markant från dag till dag, från mindre än $\pi {R_\odot}^2$ upp till flera hundra $\pi {R_\odot}^2$. Det

blev tydligt att den spekulära reflektionsmodellen inte var tillräcklig för att förklara observationerna och att ekot kan vara ett resultat av en mer komplex våg-plasma-växelverkan i den turbulenta solkoronan.

Spridning mot vågturbulens studeras rutinmässigt i laboratorier och i jonosfärsradarexperiment. De senare är mycket lika solradarexperiment, och kan således vara mycket användbara. Både jonosfären och solkoronan har magnetiska fält och densitetsgradienter. Vågturbulensen i jonosfären kan uppstå till följd av naturliga fenomen, till exempel av fältparallella strömmar, eller på konstgjord väg, till exempel då man skickar upp en högfrekvent elektromagnetisk våg, så kallade upphettningsexperiment. I solkoronan kan vågturbulensen skapas av elektronstrålar, som accelereras från solen eller från en interplanetär shock. Existensen av sådana elektronstrålar i solkoronan synliggörs genom strålning från den exciterade vågturbulensen, känd som solradioutbrott.

Rymdvädersprogrammet[1] skapade nyligen ett intresse för solradarexperiment, med det ultimata målet att tidigt kunna upptäcka massutkastningar från solkoronan som färdas mot jorden. Sådana massutkastningar kan medföra allvarliga konsekvenser för astronauters liv och hälsa, skada satelliter, samt skapa intensiva geomagnetiska stormar, som i sin tur kan leda till skador på kraftledningar och slå ut elnätet i stora områden [80]. Förslag till nya radarexperiment har till exempel givits av Thidé [87], Coles [13], och Rodriguez [78]. Det är sannolikt att nya radarobservationer med modern teknik för sändning, mottagning och signalbehandling, kombinerat med moderna UV- och röntgenobservationer kommer att bidra betydligt till vår förståelse av solens fysik.

Den här avhandlingen består av två delar. I den första delen presenterar jag översiktligt teorin och den praktiska delen av solradarexperiment. Den andra delen består av fyra artiklar som är mitt och mina kollegors bidrag till teorin om solradarexperiment.

Artikel I. Inducerad spridning från anisotropisk Langmuirturbulens med tillämpningar för solradarexperiment.

I denna artikel undersöker vi möjligheterna att med hjälp av radar påvisa anisotropisk Langmuirturbulens från en $t + l \rightleftarrows t$-process i solens korona. Vi antar att turbulensen genereras av samma elektroner som ger upphov till solradioutbrott av typ III, samt att dess vågutbredningsriktningar är kvasi- eller antiparallella med riktningen mot radarkällan. Följaktligen behandlas endast bakåtspridning. Vi använder vågkinetisk teori för att härleda uttryck för frekvensförskjutningen, spridningstvärsnittet, absorptionskoefficienten (till följd av spridning), samt det optiska djupet, vilket sammantaget leder till en uppskattning av ekospektrumet. Vi visar i) att värdet för

[1] se till exempel `http://www.spaceweather.com`

det optiska djupet kan överstiga ett, ii) att turbulensen kan ha ett stort spridningstvärsnitt ($\sigma \gg \pi {R_\odot}^2$), iii) att frekvensförskjutningarna hos den reflekterade signalen ligger i intervallen $-\omega_t/2 < \Delta\omega \lesssim -\omega_t/8$ och $\omega_t/7 \lesssim \Delta\omega \leqslant \omega_t$, där ω_t är radarfrekvensen, samt iv) att spridningsprocessens effektivitet (absorptionskoefficienten) ökar med ω_t.

Artikel II. Radardetektion av interplanetära chockvågor: spridning från anisotropisk Langmuirturbulens.

Det är väl känt att interplanetära stötvågor förknippade med massutkastningar från koronan har en betydande inverkan på magnetosfären i form av geomagnetiska stormar och substormar. Därför är det viktigt att på ett tidigt stadium kunna registrera sådana stötvågor. I denna artikel studerar vi möjligheterna till detektion av inducerad spridning från anisotropisk Langmuirturbulens, som genereras i en $t + l \rightleftarrows t$-process av elektroner som accelererats av stötvågen. Vi fokuserar på spridningsprocessens beroende av vinkeln mellan elektronstrålen och radarvågen, $\mathbf{v}_b \hat{} \mathbf{k_t}$ (i motsats till artikel I, där endast fallet $\mathbf{v}_b \hat{} \mathbf{k_t} = \pi$ behandlas). Med hjälp av vågkinetisk teori erhåller vi analytiska uttryck för absorptionskoefficienten på grund av inducerad spridning samt det optiska djupet. Dessa parametrar uppvisar ett starkt beroende av vinkeln $\mathbf{v}_b \hat{} \mathbf{k_t}$ i sönderfallsprocessen ($t \rightarrow t' + l$), medan beroendet vid koalescens ($t + l \rightarrow t'$) är svagt. På detta sätt ändras frekvensförskjutningen hos den reflekterade signalen vid sönderfall från att ligga i intervallet $-\omega_t/2 < \Delta\omega \lesssim -\omega_t/8$ vid $\mathbf{v}_b \hat{} \mathbf{k_t} = \pi$ till $0 < \Delta\omega < 0$ vid $\mathbf{v}_b \hat{} \mathbf{k_t} = \pi/2$, medan förändringen i fallet med koalescens är från $\omega_t/7 \lesssim \Delta\omega \leqslant \omega_t$ vid $\mathbf{v}_b \hat{} \mathbf{k_t} = \pi$ till $\omega_t/120 \lesssim \Delta\omega \leqslant \omega_t$ vid $\mathbf{v}_b \hat{} \mathbf{k_t} = \pi/2$. Eftersom frekvensförskjutningen måste vara av samma storleksordning som den lokala plasmafrekvensen i spridningszonen, förflyttas gränsen för spridning avsevärt i riktning mot radarkällan med ökande vinkel $\mathbf{v}_b \hat{} \mathbf{k_t}$. I detta fall sprids radarsignalen i en vinkel mot infallsriktningen, och måste därför fångas upp på stort avstånd från radarkällan. Vid transmission från jorden kan detektionen exempelvis ske med en satellit. Ett framgångsrikt experiment vid radarfrekvensen $\omega_t = 2\pi \times 100$ MHz kräver att energitätheten i turbulensen överstiger $W = 10^{-5}\, nT$, där nT är den termiska energitätheten i plasmat. Detta är enligt våra uppskattningar fullt realistiskt.

Artikel III. Spridning av radiovågor på grund av täthetsfluktuationer i solvinden samt jordens förchock.

En radiostråle från en solradar genomkorsar ett antal olika skikt på vägen mot reflektionspunkten och tillbaka: jonosfären, magnetosfären, jordens förchock och solvinden. I denna artikel uppskattar vi vinkelbreddningen hos en radarstråle till följd av täthetsfluktuationer i jordens jon- och elektronförchocker, samt i den ostörda solvinden. Energispek-

tra för täthetsvariationerna i dessa regioner fås från mätningar utförda med Clustersatelliterna. Dessa spektra används för att beräkna radiovågens vinkelbreddning i respektive område. Breddningen förväntas vara minimal i den ostörda solvinden och maximal i jonförchocken. Resultaten ger vid handen att den totala vinkelbreddningen inte bör ha någon allvarlig inverkan vid radarundersökning av solen.

Artikel IV. In situ-observationer av solradioutbrott av typ II: en ny genereringsmekanism.

Solradioutbrott av typ II hänger samman med interplanetära stötvågor som utbreder sig i rymdplasmat. Enligt gängse teorier utgör själva radioemissionen slutsteget i en hel serie av fysikaliska processer: partikelacceleration i stötvågen följs av uppkomsten av plasmavågor, vilka i sin tur omvandlas till elektromagnetiska vågrörelser (plasmaemissionsmekanismen). Slutsatserna om denna mekanism dras vanligen från fjärrobservationer av strålningen, och det råder en klar brist på in situ-observationer i källområdet. I den föreliggande artikeln redogör vi för satellitobservationer in situ av ett solradioutbrott av typ II, associerat med en interplanetär stötvåg orsakad av en massutkastning från koronan. Samtidigt med den intensiva strålningen ovan elektronplasmafrekvensen observeras subrelativistiska elektronstrålar i stötvågsfrontens omedelbara närhet. Vi föreslår att strålningen genereras lokalt vid vågfronten och precis bakom den, och presenterar en möjlig mekanism för dess uppkomst. Mekanismen involverar högenergetiska partiklar som passerar vågfronten, och är ett exempel på det som inom elektrodynamiken kallas övergångsstrålning.

8. Acknowledgments

This work has been carried out at the Department of Astronomy and Space Physics at Uppsala University as part of the LOIS project[1]. I would like to express my gratitude to all the members of the department and the staff of the Swedish Institute of Space Physics in Uppsala for the hospitality and help.

I am thankful to my supervisor Prof. Bo Thidé for help and giving me an opportunity to make this work, which was financed by the Swedish Agency for Innovation Systems VINNOVA and the Advanced Measurements and Instrumentation (AIM) graduate school.

I am deeply thankful to my supervisor Valentyn Mel'nik for giving me the lessons of the scientific school and productive mutual work. I would also like to thank the staff of the Institute of Radio Astronomy of the Ukrainian Academy of Sciences in Kharkiv for their hospitality during my visits.

I would like to thank my brother Yuri for supervising me, helping and sometimes pressing. Many thanks to Prof. Vladimir Krasnessel'skikh for his interesting ideas, and fruitful collaborative work. I am also very grateful to Prof. Vladimir Pavlenko, who was continuously teaching, helping, supporting, and inspiring me. I am thankful to Andris Vaivads for always finding time to read and correct my manuscripts and presentations, for all the help, and for wonderful fishing trips.

Last, but not least, I would like to thank my family and friends for their continuous support during this years.

[1] http://www.lois-space.net

Bibliography

[1] C. W. Allen. Interpretation of electron densities from corona brightness. *Monthl. Not. Roy. Astr. Soc.*, 107:426–432, 1947.

[2] E. V. Appleton and J. S. Hey. Solar radio noise - I. *Phil. Mag. Ser. 7*, 37:73, 1946.

[3] Melrose D. B. *Radiophys. and Quantum Electron.*, 20:945, 1977.

[4] F. G. Bass and S. Ya. Braude. On the question of reflection of radar signals off the Sun. *Ukr. Fiz. Zh.*, 2:149, 1957.

[5] Z. Bay. Reflection of microwaves from the moon. *Hungarica Acta Physica*, 1:1, 1946.

[6] A. Benz. *Plasma Astrophysics. Kinetic Processes in Solar and Stellar Coronae, second edition*. Astrophysics and Space Science Library, Vol. 279, Kluwer Academic Publishers, Dordrecht, June 2002.

[7] Arnold O. Benz and H. R. Fitze. Microwave radar observations of the Sun. *Astron. Astrophys.*, 76:354–355, 1979.

[8] M. K. Bird, M. Pätzold, P. Edenhofer, S. W. Asmar, and T. P. McElrath. Coronal radio sounding with Ulysses: Solar wind electron density near 0.1 AU during the 1995 conjunction. *Astron. Astrophys.*, 316:441–448, 1996.

[9] G. E. Brueckner, R. A. Howard, M. J. Koomen, C. M. Korendyke, D. J. Michels, J. D. Moses, D. S. Socker, K. P. Dere, P. L. Lamy, A. Lleberia, M. V. Bout, R. Schwenn, G. M. Simnett, D. K. Bedford, and C. J. Eyles. The Large Angle Spectroscopic Coronagraph (LASCO). *Solar Phys.*, 162:357–402, 1995.

[10] J. Burkepile and O. C. St. Cyr. A revised and expanded catalogue of mass ejections observed by the Solar Maximum Mission coronagraph. NCAR/TN 369, National Center for Atmospheric Research, Boluder, CO, January 1993.

[11] I. V. Chashei and V. I. Shishov. Volume scattering model for interpretation of solar radar experiments. *Solar Phys.*, 149:413, February 1994.

[12] I. V. Chashej and V. I. Shishov. The turbulence in the solar atmosphere and in the interplanetary plasma. *Astron. Zhurnal*, 61:474–482, June 1984.

[13] W. A. Coles. Solar radar. In D. E. Gary and C. U. Keller, editors, *Solar and Space Weather Radiophysics - Current Status and Future Developments*, number 314 in Astrophysics and Space Science Library, page chap. 16. Kluwer Academic Publishers, Dordrecht, 2004.

[14] R. C. Davidson. *Methods in Nonlinear Plasma Theory*. Academic Press, 1972.

[15] V. Domingo, B. Fleck, and A. I. Poland. The SOHO mission: An overview. *Solar Phys.*, 162:1–37, 1995.

[16] V. R. Eshleman. In J. Aarons, editor, *Solar System Radio Astronomy*, page 292. Plenum, 1965.

[17] V. R. Eshleman. Radar Astronomy. *Science*, 158:585, November 1967.

[18] V. R. Eshleman, R. C. Barthle, and P. B. Gallagher. Radar Echoes from the Sun. *Science*, 131:329, February 1960.

[19] J. V. Evans. Radar Studies of Planetary Surfaces. *Ann. Rev. of Astron. and Astrophys.*, 7:201–248, 1969.

[20] H. R. Fitze and A. O. Benz. The microwave solar radar experiment. I - Observations. *Astrophys. J.*, 250:782, November 1981.

[21] D. E. Gary and C. U. Keller. *Solar and Space Weather Radiophysics - Current Status and Future Developments*. Solar and Space Weather Radiophysics - Current Status and Future Developments. Edited by Dale E. Gary, Center for Solar-Terrestrial Research, New Jersey Institute of Technology, Newark, N.J., U.S.A.; Christoph U. Keller, National Solar Observatory, Tucson, AZ, U.S.A. ASTROPHYSICS AND SPACE SCIENCE LIBRARY Volume 314 Kluwer Academic Publishers, Dordrecht, September 2004.

[22] N. N. Gerasimova. Comparison of the results of radar studies of the solar corona and solar activity. *Astron. Zhurnal*, 51:813, August 1974.

[23] V. L. Ginzburg. Solar Emission in the Radiofrequency Range. *R.C. (Doklady) Acad. Sci. USSR*, 52:487, 1946.

[24] V. L. Ginzburg. *Theoretical physics and astrophysics*. International Series in Natural Philosophy, Oxford: Pergamon, 1979, 1979.

[25] V. L. Ginzburg and I. M. Frank. Radiation of a uniform moving electron due to its transition from one medium into another. *J. Phys. (Moscow)*, 9:353, 1945.

[26] V. L. Ginzburg and V. N. Tsytovich. Several problems of the theory of transition radiation and transition scattering. *Phys. Rep.*, 49:1–89, January 1979.

[27] V. L. Ginzburg and V. V. Zhelezniakov. On the Possible Mechanisms of Sporadic Solar Radio Emission (Radiation in an Isotropic Plasma). *Soviet Astronomy*, 2:653, October 1958.

[28] Vitaliy L. Ginzburg. *The Propagation of Electromagnetic Waves in Plasmas*. Pergamon Press, Oxford, second, revised and enlarged edition, 1970.

[29] M. V. Goldman, G. F. Reiter, and D. R. Nicholson. Radiation from a strongly turbulent plasma - Application to electron beam-excited solar emissions. *Physics of Fluids*, 23:388–401, February 1980.

[30] I. M. Gordon. Interpretation of Radio Echoes from the Sun. *Astrophys. Lett.*, 2:49, 1968.

[31] I. M. Gordon. Radar Observations of the Sun, and a Mechanism for Producing the Reflected Signal in the Corona. *Astron. Zhurnal*, 45:1002, 1968.

[32] I. M. Gordon. Radar Explorations of the Sun and Physical Processes of the Solar Corona. *Astrophys. Lett.*, 3:181, 1969.

[33] I. M. Gordon. Radar Research of the Sun and Cosmic Plasma Turbulence. *IRE doct. fiz. mat. nauk thesis, Kharkov*, 1971.

[34] I. M. Gordon. Plasma theory of radio echoes from the Sun and its implications for the problem of the solar wind. *Space Sci. Rev.*, 15:157, 1973.

[35] I. M. Gordon, V. A. Liperovskii, and V. N. Tsytovich. Turbulence Spectra of the Solar Coronal Plasma and the Structure of a Radar Signal. I. *Soviet Astronomy*, 15:54, August 1971.

[36] J. T. Gosling. Coronal mass ejections: An overview. In Joann Joselyn Nancy Crooker and Joan Feynman, editors, *Coronal Mass Ejections*, Geophysical Monograph 99, pages 9–16. American Geophysical Union, Washington DC, 1997.

[37] J. T. Gosling, D. J. McComas, J. L. Phillips, and S. J. Bame. Geomagnetic activity associated with earth passage of interplanetary shock disturbances and coronal mass ejections. *J. Geophys. Res.*, 96(A5):7831–7839, 1991.

[38] Wilhelm Hanle. Uber magnetische Beeinflssung der Polarisation der Resonanzfluoreszenz. *Z. Phys.*, 30:93–105, 1924.

[39] R. A. Howard, G. E. Brueckner, O. C. St. Cyr, D. A. Biesecker, K. P. Dere, M. J. Koomen, C. M. Korendyke, P. L. Lamy, A. Llebaria, M. V. Bout, D. J. Michels, J. D. Moses, S. E. Paswaters, S. P. Plunkett, R. Schwenn, G. M. Simnett, D. G. Socker, S. J. Tappin, and D. Wang. Observations of CMEs from SOHO/LASCO. In Joann Joselyn Nancy Crooker and Joan Feynman, editors, *Coronal Mass Ejections*, Geophysical Monograph 99, pages 17–26. American Geophysical Union, Washington DC, 1997.

[40] B. Isham, C. La Hoz, M. T. Rietveld, T. Hagfors, and T. B. Leyser. Cavitating Langmuir Turbulence Observed during High-Latitude Ionospheric Wave Interaction Experiments. *Physical Review Letters*, 83:2576–2579, September 1999.

[41] J. C. James. Radar echoes from the sun. *IEEE Trans. Mil. Elect.*, MIL-8:210–225, July–October 1964. Identical to *IEEE Trans. Antennas Propagat.*, *AP-12*, 876-891.

[42] J. C. James. Some Observed Characteristics of Solar Radar Echoes and Their Implications. *Solar Phys.*, 12:143, 1970.

[43] S. Kahler, D. V. Reames, N. R. Sheeley, Jr., R. A. Howard, D. J. Michels, and M. J. Koomen. A comparison of solar helium-3-rich events with type II bursts and coronal mass ejections. *Astrophys. J.*, 290:742–747, March 1985.

[44] S. W. Kahler. Solar flares and coronal mass ejections. *Ann. Rev. Astron. Astrophys.*, 30:113–141, 1992.

[45] Anatoliy Karashtin, V. Fridman, and O. Sheiner. Private communication, 2002.

[46] Anatoliy N. Karashtin, G. P. Komrakov, Yuriy V. Tokarev, and Yu. V. Shlyugaev. Radar studies using the SURA facility. *Radiophys. Quant. Electronics*, 42(8):674–686, 1999.

[47] Anatoliy N. Karashtin, Gregori P. Komrakov, Yuriy V. Tokarev, and Yuriy V. Shlugaev. Solar monostatic radio sounding at the SURA facility. In *VII Russian-UIS Symposium on Solar-Terrestrial Physics, Book of Abstracts*, pages 24–25, Moscow, Dec 15-18 1998.

[48] F. J. Kerr. *Proc. IRE*, 40:660, 1952.

[49] M. V. Khotyaintsev, V. N. Mel'Nik, B. Thidé, and O. O. Konovalenko. Combination Scattering by Anisotropic Langmuir Turbulence with Application to Solar Radar Experiments. *Solar Phys.*, 234:169–186, March 2006.

[50] E. N. Kruchina, R. Z. Sagdeev, and V. D. Shapiro. Strong Langmuir turbulence as a source of radio emission. *Journal of Experimental and Theoretical Physics Letteres*, 32:419, September 1980.

[51] K. R. Lang. *Sun, Earth and Sky*. Springer-Verlag, Berlin, 1995. ISBN 3-540-58778-0.

[52] K. R. Lang. *The Sun from Space*. Springer-Verlag, Berlin, 2000.

[53] R. M. MacQueen, A. Csoeke-Poecke, E. Hildner, R. Reynolds, A. Stanger, H. Te Poel, and W. J. Wagner. The High Altitude Observatory coronagraph/polarimeter on the Solar Maximum Mission. *Solar Phys.*, 65:91–107, 1980.

[54] R. M. MacQueen, J. A. Eddy, J. T. Gosling, E. Hildner, R. H. Munro, G. A. Newkirk, A. I. Poland, and C. L. Ross. The outer corona as observed from Skylab. *Astrophys. J. Lett.*, 187:L85–L88, 1974.

[55] Gottfired Mann, F. Jensen, R. J. MacDowall, M. L. Kaiser, and R. G. Stone. A heliospheric density model and type III radio bursts. *Astron Astrophys.*, 348:614–620, 1999.

[56] D. J. McLean and N. R. Labrum. *Solar radiophysics: Studies of emission from the sun at metre wavelengths*. Solar Radiophysics: Studies of Emission from the Sun at Metre Wavelengths, 1985.

[57] V. N. Mel'nik. Plasma theory of radar signal reflection from the Sun. 1. Processes of scattering off anisotropic Langmuir turbulence. *Radiofizika i Radioastronomija*, 3:12, 1998.

[58] V. N. Mel'nik. On the plasma theory of reflection of a radar signal from the sun. *Astronomy Letters*, 25:336, May 1999.

[59] V. N. Mel'nik. Radar scattering by anisotropic Langmuir turbulence. *Solar Phys.*, 184:363, February 1999.

[60] V. N. Mel'nik. Plasma theory of solar radar echoes. *Radio Sci.*, 38:2–1, May 2003.

[61] V. N. Mel'nik, A. A. Konovalenko, H. O. Rucker, A. A. Stanislavsky, E. P. Abranin, A. Lecacheux, G. Mann, A. Warmuth, V. V. Zaitsev, M. Y. Boudjada, V. V. Dorovskii, V. V. Zaharenko, V. N. Lisachenko, and C. Rosolen. Observations of Solar Type II bursts at frequencies 10-30 MHz. *Solar Phys.*, 222:151–166, July 2004.

[62] V. N. Mel'nik, V. Lapshin, and E. Kontar. Propagation of a Monoenergetic Electron Beam in the Solar Corona. *Solar Phys.*, 184:353, February 1999.

[63] D. B. Melrose. Mode coupling in the solar corona. VI - Direct conversion of Langmuir waves into o-mode waves. *Australian Journal of Physics*, 33:121–137, March 1980.

[64] D. B. Melrose. The emission mechanisms for solar radio bursts. *Space Science Reviews*, 26:3–38, May 1980.

[65] D. B. Melrose. Plasma emission - A review. *Solar Phys.*, 111:89–101, 1987.

[66] D. B. Melrose. Collective plasma radiation processes. *Ann. Rev. of Astron. and Astrophys.*, 29:31–57, 1991.

[67] D. J. Michels, R. A. Howard, M. J. Koomen, and Jr. N. R. Sheeeley. Satellite observations of the outer corona near sunspot maximum. In Mukul R. Kundu and T. E. Gergely, editors, *Radio Physics of the Sun*, page 439. D. Reidel Publ. Co., Hingham, MA, 1980.

[68] J. Mofensen. Radar echoes from the moon. *Electronics*, 19:92, 1946.

[69] L. Muschietti. Electron beam formation and stability. *Solar Phys.*, 130:201–228, December 1990.

[70] Marcia Neugebauer and Raymond Goldstein. Particle and field signatures of coronal mass ejections in the solar wind. In Joann Joselyn Nancy Crooker and Joan Feynman, editors, *Coronal Mass Ejections*, Geophysical Monograph 99, pages 245–251. American Geophysical Union, Washington DC, 1997.

[71] G. J. Newkirk. The Solar Corona in Active Regions and the Thermal Origin of the Slowly Varying Component of Solar Radio Radiation. *Astrophys. J.*, 133:983, May 1961.

[72] J. E. Ohlsen. Sci. rep. no. 21. Technical report, Stanford Electric Lab., Stanford, 1967.

[73] Alan Parrish. Solar radar experiments, 1967. Technical Report 300, Center for Radiophysics and Space Research, Cornell University, Ithaca, New York, April 1968.

[74] E. R. Priest. *Solar Magnetohydrodynamics*. Reidel, 1982.

[75] V. M. Razmanov, A. I. Efimov, and O. I. Iakovlev. Radio-signal spectral line formation during propagation in the circumsolar plasma. *Radiofizika*, 22:1051–1060, 1979.

[76] M. T. Rietveld, P. N. Collis, and J.-P. St.-Maurice. Naturally enhanced ion acoustic waves in the auroral ionosphere observed with the EISCAT 933-MHz radar. *J. Geophys. Res.*, 96:19291, November 1991.

[77] P. Rodriguez. Radar studies of the solar corona: A review of experiments using HF wavelengths. In K. S. Balasubramaniam, S. L. Kiel, and R. N. Smartt, editors, *Radio Astronomy at Long Wavelengths*, volume Geophysical Monograph 119, pages 155–165. American Geophysical Union, 2000.

[78] P. Rodriguez. Solar radar astronomy with the low-frequency array. *Plan. and Space Sci.*, 52:1391, December 2004.

[79] Paul Rodriguez, A. Konovalenko, O. Ulyanov, Lev M. Erukhimov, Yu. Belov, Yu. Tokarev, Anatoliy Karashtin, and K. van't Klooster. Detection of HF radar reflection from the solar corona. In *Transactions of the AGU, EOS Supplemental Issue*, volume 78, page F538. American Geophysical Union, 1997. (Paper SH21A-15, AGU Fall Meeting, San Fransisco, CA, December 8–12, 1997).

[80] L. Rosenqvist, H. Opgenoorth, S. Buchert, I. McCrea, O. Amm, and C. Lathuillere. Extreme solar-terrestrial events of October 2003: High-latitude and Cluster observations of the large geomagnetic disturbances on 30 October. *Journal of Geophysical Research (Space Physics)*, 110:9, September 2005.

[81] S. M. Rytov, Yu. A. Kravtsov, and V. I. Tatarskii. *Principles of Statistical Radiophysics*, volume 4. Springer-Verlag, 1989.

[82] P. A. G. Scheuer. The absorption coefficient of a plasma at radio frequencies. *Monthly Notices of the Royal Astron. Society*, 120:231, 1960.

[83] P. Song, H. J. Singer, and G. L. Siscoe, editors. *Space Weather*. Geophysical Monograph 125. American Geophysical Union, Washington DC, 2001.

[84] P. A. Sturrock. Type III Solar Radio Bursts. In W. N. Hess, editor, *The Physics of Solar Flares*, page 357, 1964.

[85] T. Takakura. Numerical simulation of type III solar radio bursts caused by high-density electron beam. *Solar Phys.*, 62:383–391, June 1979.

[86] G. Thejappa, D. Lengyel-Frey, R. G. Stone, and M. L. Goldstein. Evaluation of Emission Mechanisms at omega P E Using ULYSSES Observations of Type III Bursts. *Astrophys. J.*, 416:831, October 1993.

[87] Bo Thidé. Radio research and large low frequency array telescopes. In B. Nilsson and L. Fishman, editors, *Mathematical Modelling of Wave Phenomena*, number 7 in Mathematical Modelling in Physics, Engineering and Cognitive Science, pages 315–331. Växjö University Press, Dordrecht, 2002.

[88] R. Tousey. The solar corona. In M. J. Rycroft and S. K. Runcorn, editors, *Space Research XIII*, pages 713–730. Akademie-Verlag, Berlin, 1973.

[89] V. N. Tsytovich. *Nonlinear Effects in Plasma*. New York: Plenum Press, 1970.

[90] G. Leonard Tyler, Joseph P. Brenkle, Thomas A. Komarek, and Arthur I. Zygielbaum. The viking solar corona experiment. *J. Geopys. Res.*, 82(28):4335–4340, 1977.

[91] J. M. Weisberg, J. M. Rankin, R. R. Payne, and C. C. Counselmann. Further changes in the distribution of density and radio scattering in the solar corona in 1973. *Astrophys. J.*, 209:252–258, 1976.

[92] D. G. Wentzel. A New Interpretation of James's Solar Radar Echoes Involving Lower-Hybrid Waves. *Astrophys. J.*, 248:1132, 1981.

[93] Richard Woo. Mass ejections observed in radio propagation measurements through the solar corona. In Joann Joselyn Nancy Crooker and Joan Feynman, editors, *Coronal Mass Ejections*, Geophysical Monograph 99, pages 235–244. American Geophysical Union, Washington DC, 1997.

[94] Vladimir V. Zheleznyakov. *Radio Emission of the Sun and the Planets*. Pergamon Press, Oxford, 1970.

Acta Universitatis Upsaliensis

Digital Comprehensive Summaries of Uppsala Dissertations from the Faculty of Science and Technology 231

Editor: The Dean of the Faculty of Science and Technology

A doctoral dissertation from the Faculty of Science and Technology, Uppsala University, is usually a summary of a number of papers. A few copies of the complete dissertation are kept at major Swedish research libraries, while the summary alone is distributed internationally through the series Digital Comprehensive Summaries of Uppsala Dissertations from the Faculty of Science and Technology. (Prior to January, 2005, the series was published under the title "Comprehensive Summaries of Uppsala Dissertations from the Faculty of Science and Technology".)

Distribution: publications.uu.se
urn:nbn:se:uu:diva-7192

ACTA
UNIVERSITATIS
UPSALIENSIS
UPPSALA
2006